A STUDY OF LOCALIZED WAVES AND THEIR APPLICATION TO MEDICAL ULTRASOUND IMAGING

By

Linda Bie

B. A. Sc. (Engineering Physics) University of British Columbia, 1991

B. Sc. (Mathematics/Physics) University of British Columbia, 1989

A THESIS SUBMITTED IN PARTIAL FULFILLMENT OF

THE REQUIREMENTS FOR THE DEGREE OF

MASTER OF APPLIED SCIENCE

in

THE FACULTY OF GRADUATE STUDIES

DEPARTMENT OF ELECTRICAL ENGINEERING

We accept this thesis as conforming

to the required standard

THE UNIVERSITY OF BRITISH COLUMBIA

April 1994

In presenting this thesis in partial fulfilment of the requirements for an advanced degree at the University of British Columbia, I agree that the Library shall make it freely available for reference and study. I further agree that permission for extensive copying of this thesis for scholarly purposes may be granted by the head of my department or by his or her representatives. It is understood that copying or publication of this thesis for financial gain shall not be allowed without my written permission.

Department of Electrical Engineering
The University of British Columbia
2075 Wesbrook Place
Vancouver, Canada
V6T 1W5

Date: April 28, 1994

Abstract

A study of localized waves and their potential for application to medical ultrasound imaging is conducted using analytical and numerical simulation techniques. Simulated focused ultrasound fields representing approximations to the focus wave modes and modified power spectrum pulses are generated from synthesized, two-dimensional arrays. The results in terms of attenuation and diffraction are compared with previously published data for continuous waves and X waves, which are another localized wave solution.

Through the course of simulations different array sizes and source element densities are examined to determine the consequent effects on the generated localized waves. Array size determines the distance to which the wave will propagate while source element density affects the smoothness or amount of error in the reconstruction. In addition, the effect of 'folding' is examined and found to reduce attenuation but to have little effect on beam waist width within the depth of interest for medical ultrasound imaging (up to $0.4m$). Introducing folding terms increases substantially the complexity and magnitude of the required source waveforms.

Pure focus wave mode beams are found to differ insignificantly from the modified power spectrum pulse when generated by a finite array. Simulations show that for a square source array as small as nine by nine elements with element spacing $5.5mm$, the lateral beam half-width (at the $1/e$ point) at $30cm$ depth penetration in water is only $10mm$, and the depth of field, defined as the distance where the wave falls to half its original magnitude, is $405mm$. This is a substantial improvement over continuous waves—on the order of 23% for the beam half-width—and is comparable to results reported for X waves launched from a circular array with the same area.

Table of Contents

List of Figures

Acknowledgment

A debt of gratitude is owed to my thesis supervisor, Dr. Matthew R. Palmer, for his contribution to this work. I would also like to thank everybody else who read and offered comments on my work in progress. Finally, I wish to thank my friends and family, especially my parents Lyle and Faye Bie, for their support throughout this endeavor.

Chapter 1

Introduction

Ultrasound imaging is used in many areas. In industry it is used to perform non-destructive testing, geologists use it to examine subterranean structures, but probably the most widely-known use is in medicine. Over the past few years, medical applications have expanded considerably. A major advantage ultrasound has over many other types of medical imaging is that it does not use ionizing radiation, which is believed to make it relatively safe. So far, exposure to ultrasound at diagnostic levels has not been linked to any harmful effects (Hykes et al., 1992, p. 204). Diagnostic, as opposed to therapeutic, uses of ultrasound include obstetrics, cardiac imaging, detection of mid-line shift following head trauma, localization of foreign bodies in the eye, and evaluation of abdominal masses.

In the most common ultrasound modes[1], the image is composed of reflected rather than transmitted waveforms. The incident wave is reflected back to the transducer at reflective interfaces. The intensity of the reflected wave is a measure of the reflectivity of the interface, and the time required for the round trip is a measure of the depth of the interface. Soft tissue interfaces are weakly reflective, so the amplitude of the returning waves is small. Also, waves are attenuated due to divergence, absorption, diffraction, scattering, and refraction. Diffractive spreading is responsible for a major reduction in resolution, making it one of the most limiting factors in attaining a high quality

[1]The different configurations used in ultrasound imaging are referred to as 'modes'. For a description of these modes see *Ultrasound Physics and Instrumentation* (Hykes et al., 1992) or *Medical Imaging Systems* (Macovski, 1983).

image. Attempts have been made to compensate for diffraction, such as mechanically or electronically focusing the wave, but these measures bring a different set of problems. The poor image quality, especially the problem with resolution, means that ultrasound is restricted to qualitative use. The introduction of a more suitable, robust wave which does not suffer diffractive spreading would alleviate some of the image quality problems. Specifically, if resolution can be improved, it may be possible to use ultrasound for quantitative analysis, thereby making it a more powerful diagnostic tool.

There have been attempts made to use transmitted rather than reflected waves in ultrasound imaging, where the transmitting and receiving transducers rotate around the patient opposite each other, much like x-ray computed tomography (CT) scanning. The image is reconstructed using the same techniques as for CT scans. For imaging in many areas of the body, this type of scanning is not feasible, since highly reflective interfaces such as tissue-bone or tissue-gas result in a transmitted wave with very low intensity, which causes detection problems. In bodily structures that are more uniform, such as in the detection of breast cancer, tomographic ultrasound could be useful (Hykes et al., 1992, p. 78). It is with this type of ultrasound imaging that the greatest success with quantitative imaging has been experienced (Greenleaf, 1983).

In designing an ultrasound wave, desirable qualities are that the wave be unidirectional, uniform in intensity, and of limited spatial dimensions for good spatial resolution. Over the past decade, new solutions to the scalar wave equation have been reported which suggest the existence of highly focused waves. These waves retain their compact, focused shape over great distances, that is, they don't suffer diffractive spreading like the continuous waves now used. They exhibit an extended depth of field, which makes them ideal for ultrasound imaging (Lu and Greenleaf, 1992b; Fatemi and Arad, 1992). They can be created using a two-dimensional array of transducers, with each element in the array being independently addressable. The size of the array and the spacing between

the array elements are critical in the generation of these waves. If an array of suitable size and element spacing, with independently addressable elements, can be manufactured, localized waves could be launched and applied to ultrasound imaging, potentially producing a better, higher resolution image than is currently available.

The focus of this work will be to study localized waves and their potential application to medical ultrasound imaging. Attention will be focused on two versions of localized waves, the original focus wave mode (FWM) introduced by Brittingham, (Brittingham, 1983), and the modified power spectrum (MPS) pulse proposed by Ziolkowski, (Ziolkowski, 1985). The FWM has finite energy density but infinite energy, and will propagate to infinity without decay. It was believed that the infinite energy nature of the FWM was a barrier to launching these waves, so researchers set out to find finite energy variations of this solution. The MPS pulse is a finite energy pulse derived from the FWM which has the addition of a multiplicative term that causes $1/r$ decay after an extended period of propagation.

Ziolkowski later proposed a method to launch the MPS pulse using a two-dimensional array of transducers (Ziolkowski, 1989). This launching scheme is based on an integral formulation over an infinite surface, so to create a perfect pulse using this method, an array of infinite size with infinitely fine (effectively continuous) element spacing is required, although approximations to the pulse can be launched from a finite array with discrete elements. With the introduction of the array launching scheme came research into overcoming shortcomings produced by truncating the array and discretizing the elements. Ziolkowski introduced a mapping which 'folded' points in the source plane which are outside the array to points inside the array (Ziolkowski, 1989). When the elements are excited with the folded source function, the array should behave like one which is larger.

The characteristics and limitations of localized waves generated from a finite, discrete

array of transducers will be examined through computer simulation. The effects of different array properties will be examined, including array size and element spacing. It is expected that a large, dense array will produce a better approximation to a localized wave than a smaller, sparse array. A description of exactly how truncation and sampling rate affect the reconstruction is sought. The use of Ziolkowski's folding scheme will be investigated. Although folding makes the array act like one which is larger, the effective element spacing between the folded elements increases, which will exaggerate the detrimental effects of a non-continuous sampling rate. Both the benefits and the cost of incorporating this scheme will be explored.

The FWM and MPS pulses will be used in these simulations. The same array launching method proposed to generate the MPS pulse will be applied to the FWM formulation. The infinite energy nature of the FWM should not be a problem, because it is being launched from a finite array. The waves generated by a finite, discrete array are only approximations to the intended wave, and it is the array which determines the energy and propagation characteristics. The finiteness of the array should override the infinite energy nature of the FWM pulse. Since the array probably determines the propagation characteristics, it seems sensible to start with the 'perfect' FWM rather than the MPS pulse which has its own decay behavior built in. There are limitations caused by the array, so there should be no need to have limitations in the wave function.

Comparisons will be made between the localized waves discussed in this paper and the currently used continuous wave, as well as another limited diffraction beam, the X wave. The localized waves should perform better than the continuous waves, in that they should propagate farther without diffracting, and comparably to the X waves.

Chapter 2

Background

2.1 Localized Waves

Focus wave modes (FWM) were first proposed by Brittingham (Brittingham, 1983). He was searching for electromagnetic pulses which were solutions to the homogeneous Maxwell's equations, continuous and non-singular with a three-dimensional pulse structure, and nondispersive for all time. They also were to move at light velocity in straight lines and carry finite energy. His solutions met all these criteria but the last. Although they had finite energy density, they carried infinite energy. Brittingham's work spurred activity in finding packet-like solutions, resulting in theories for nondiffracting beams (Durnin et al., 1987; Durnin, 1987), electromagnetic missiles (Wu, 1985; Wu et al., 1987), focus wave modes (Hillion, 1986), X waves (Lu and Greenleaf, 1992a; Lu et al., 1993), and the modified power spectrum pulse (Ziolkowski, 1985; Ziolkowski, 1989).

An elegant relation between the original FWM's and solutions of the homogeneous, free-space wave equation, ψ_h was put forth by Palmer and Donnelly (Palmer and Donnelly, 1993), and will be reiterated here. The governing wave equation is:

$$\left(\nabla^2 - \frac{1}{c^2}\frac{\partial^2}{\partial t^2}\right)\psi_h = 0 \tag{2.1}$$

where c is the wave propagation speed. Assuming the direction of propagation is along the z axis, and substituting the characteristic variables $u = z - ct$ and $v = z + ct$, gives

the following form for Equation (2.1):

$$\left(\nabla_{\perp}^2 + 4\frac{\partial^2}{\partial u\,\partial v}\right)\psi_h = 0 \tag{2.2}$$

where $\nabla_{\perp}^2$ is the transverse differential operator, in this case $\partial^2/\partial x^2 + \partial^2/\partial y^2$. A class of functions which solve Equation (2.2) is given by:

$$\psi_h = \frac{1}{u-u_0} f\left(v + \frac{\rho^2}{u-u_0}\right) \tag{2.3}$$

where f is an arbitrary twice differentiable function, ρ is the transverse distance, and u_0 is an arbitrary constant. Consider the case $f(\xi) = e^{ik\xi}$, where k is a real constant. Substituting into Equation(2.3) yields:

$$\psi_k = \frac{1}{u-u_0} e^{ikv} e^{\frac{ik\rho^2}{u-u_0}} \tag{2.4}$$

Setting the constant $u_0 = iz_0$, where z_0 is real gives, except for a multiplicative constant, the FWM solution introduced by Ziolkowski which represents a modulated, moving Gaussian pulse (Ziolkowski, 1985).

$$\phi_k = \frac{-1}{4\pi}\psi_k = \frac{1}{4\pi i(z_0+iu)} e^{ikv} e^{\frac{-k\rho^2}{z_0+iu}} = \frac{1}{4\pi i[z_0+i(z-ct)]} e^{ik(z+ct)} e^{\frac{-k\rho^2}{z_0+i(z-ct)}} \tag{2.5}$$

The value of kz_0 must be positive, in order for the solutions to be bounded as $\rho \to \infty$. The FWM with parameters $z_0 = 4.5 \times 10^{-4} m$ and $k = 2m^{-1}$ is shown in Figure 2.1.

At the pulse center, that is, for $z = ct$, the intensity of the Gaussian pulse-like FWM decreases with the distance from the axis of propagation as $e^{-k\rho^2/z_0}$. So, the parameters k and z_0 determine the localization to the z axis. Small values of k/z_0 produce pulses which look like transverse plane waves while large values yield highly localized particle-like solutions. The pulse is also localized along the axis of propagation, as away from the pulse center on this axis its amplitude decays as $1/\sqrt{(z_0^2 + (z-ct)^2)}$. As with Brittingham's solutions, these pulses have finite energy density but infinite energy. They will propagate without decay at the pulse center infinitely, oscillating with period π/k.

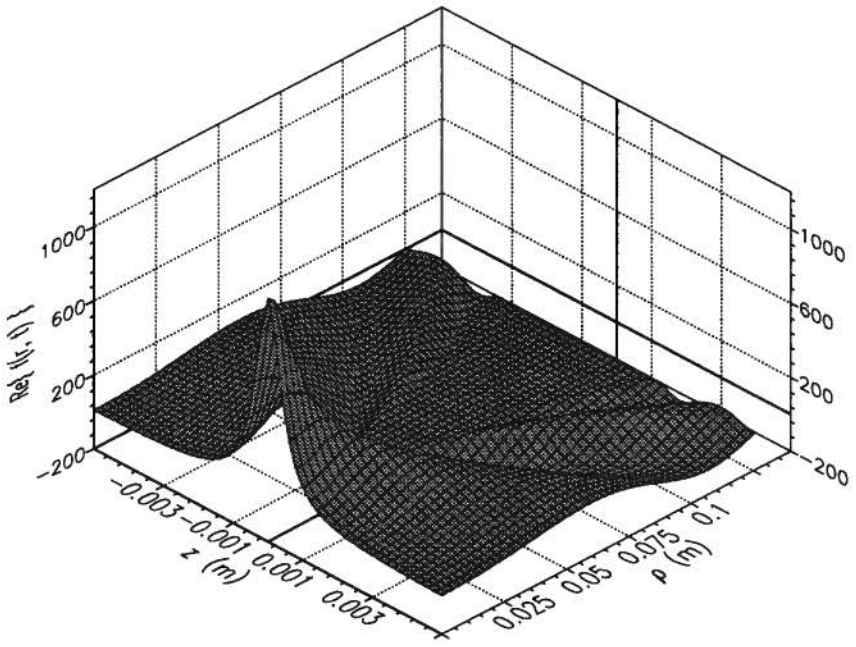

Figure 2.1: The FWM at the origin for parameters $z_0 = 4.5 \times 10^{-4} m$ and $k = 2m^{-1}$.

It was thought that in order to be useful, these theoretical pulses must be made physically realizable and therefore of finite energy. The infinite energy solutions of Equation(2.5) can be used as a basis to construct finite energy solutions (Ziolkowski, 1985). The following function is a superposition over k with weighting function $F(k)$, so it also solves the wave equation.

$$\begin{aligned} f(\vec{r},t) &= \int_{-\infty}^{\infty} \phi_k(\vec{r},t) F(k) dk \\ &= \frac{1}{4\pi i[z_0 + i(z-ct)]} \int_0^{\infty} F(k) e^{-ks} dk \end{aligned} \tag{2.6}$$

where

$$s = s(\rho, z, t) = \frac{\rho^2}{z0 + i(z-ct)} - i(z+ct) \tag{2.7}$$

This superposition will produce a finite energy solution if $F(k)$ satisfies:

$$\int_0^\infty |F(k)|^2 \frac{1}{k} dk < \infty \tag{2.8}$$

as shown in (Ziolkowski, 1989).

The function $f(\vec{r}, t)$ in Equation(2.6) has the form of a Laplace transform, leading to the conclusion that further interesting solutions can be found by consulting a table of Laplace transforms. In this way, Ziolkowski's modified power spectrum (MPS) pulse was developed. It is so named because the chosen spectrum is a scaled and truncated version of the power spectrum, $F_{ps}(k) = k^{\alpha-1}e^{-ak}$.

$$F_{mps}(k) = \begin{cases} 4\pi i\beta \dfrac{(\beta k - b)^{\alpha-1} e^{-a(\beta k - b)}}{\Gamma(\alpha)} & k > \dfrac{b}{\beta} \\ 0 & 0 \le k < \dfrac{b}{\beta} \end{cases} \tag{2.9}$$

The form of the MPS pulse is:

$$f(\vec{r}, t) = \frac{1}{z_0 + i(z - ct)} \frac{1}{(s/\beta + a)^\alpha} e^{-\frac{bs}{\beta}} \tag{2.10}$$

where $s = s(\rho, z, t)$ is given in Equation(2.7). Figure 2.2 shows the MPS pulse at the origin for parameters $a = 1.0m$, $\alpha = 1.0$, $b = 600m^{-1}$, $\beta = 300$, and $z_0 = 4.5 \times 10^{-4}m$. The speed of sound in water is $c = 1.5 \times 10^3 m/s$.

The values of the parameters a, b, α, β, and z_0 can be altered to produce a wave with the desired characteristics. For example, if z_0 is decreased, the center frequency of the pulse is increased, but the localization to the z-axis is decreased. The decrease in localization can be countered by increasing the value of b or decreasing β since all three parameters affect the degree of localization.

To examine the behavior of the wave along the direction of propagation, $\hat{z}$, at the pulse center, consider the case where $\alpha = 1$, $\beta \gg 1$ $(1/\beta z_0 \ll 1)$, $\rho = 0$, and $z = ct$. The

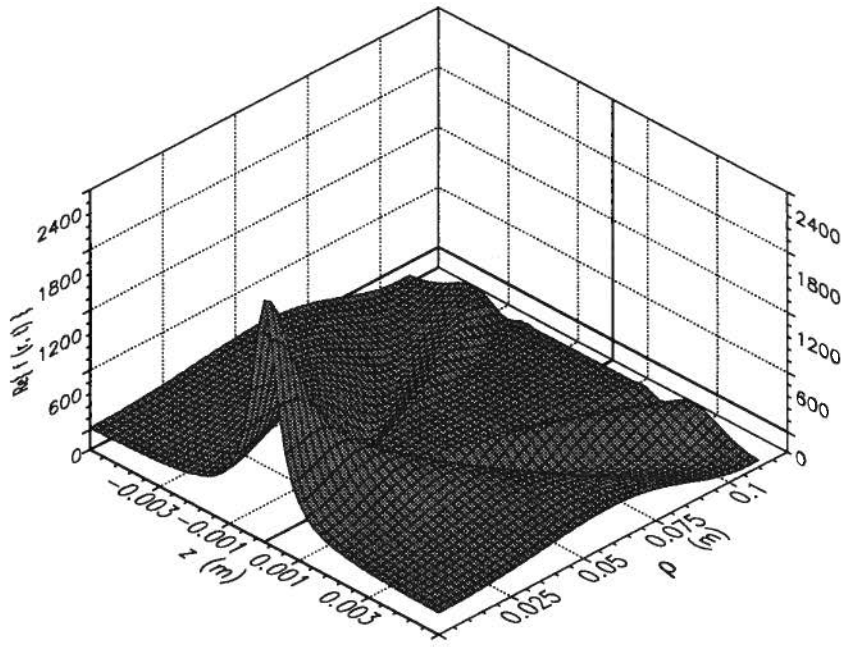

Figure 2.2: The MPS pulse at the origin for parameters $a = 1.0m$, $\alpha = 1.0$, $b = 600m^{-1}$, $\beta = 300$, and $z_0 = 4.5 \times 10^{-4}m$.

real part of the MPS pulse is given by:

$$\Re\{f(\rho = 0, z = ct)\} = \frac{1}{az_0} \frac{1}{1 + \left(\frac{2z}{a\beta}\right)^2} \left(\cos\left(\frac{2bz}{\beta}\right) - \frac{2z}{a\beta} \sin\left(\frac{2bz}{\beta}\right) \right) \tag{2.11}$$

In the region where $z \ll \beta/2b$ and $z < a\beta/2$, the value of the function at the pulse center is constant at $1/az_0$. When $z > \beta/2b$ and $z < a\beta/2$, the $\cos(2bz/\beta)$ term dominates, so the pulse becomes oscillatory with period of oscillation $\pi\beta/b$. When $z > a\beta/2$, the function decays as $1/z$. By choosing a very large value for β, this decay behavior can be made to occur arbitrarily far from the origin. The behavior of the pulse along the direction of propagation is illustrated in Figure 2.3.

The MPS pulse is like the FWM but with the addition of the term which brings about the $1/z$ decay, so, in the range $z < a\beta/2$ at least, the localization properties for the two

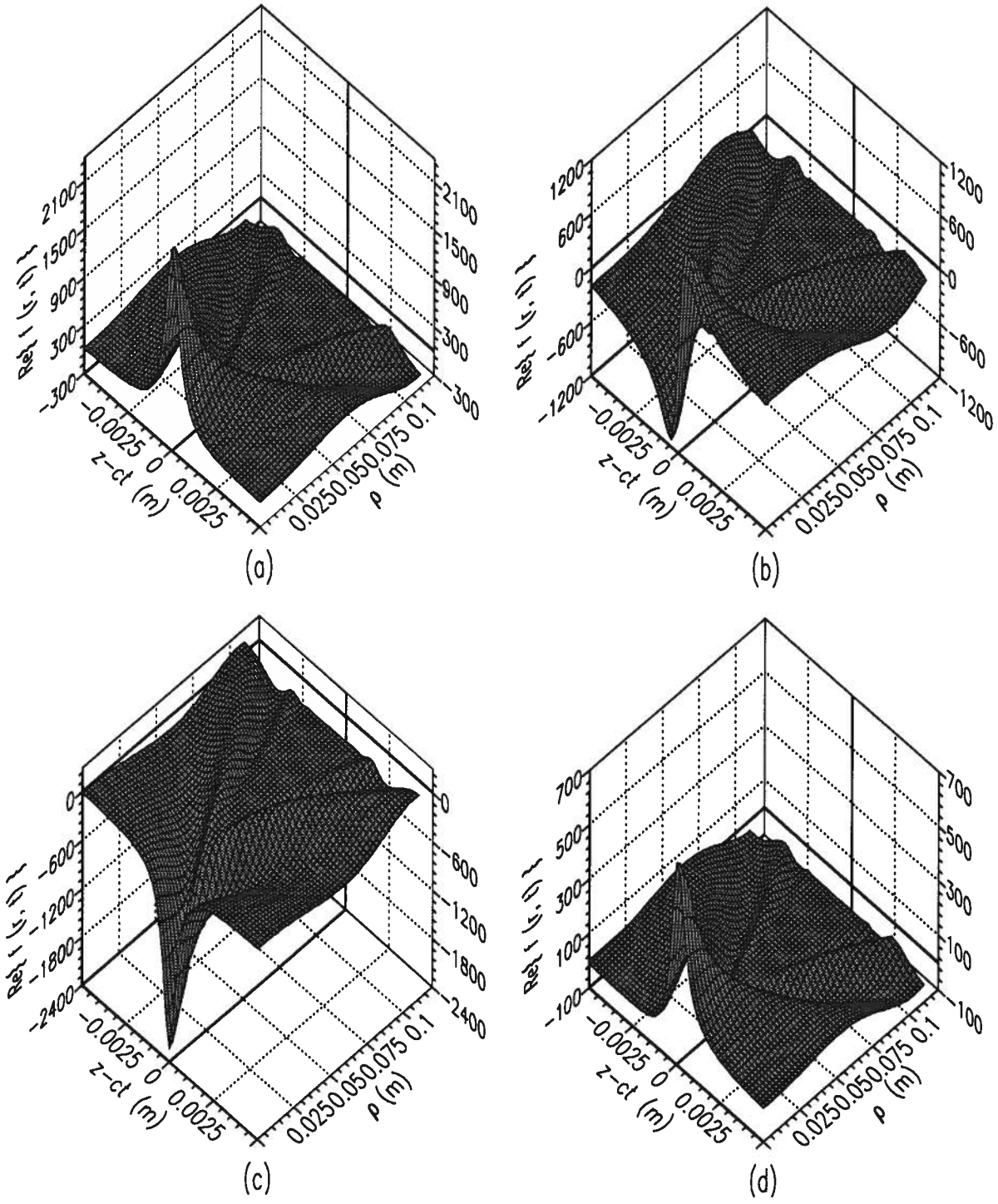

Figure 2.3: The MPS pulse at distances (a) $\pi\beta/b$, (b) $5\pi\beta/4b$, (c) $3\pi\beta/2b$, and (d) $\pi a\beta(\beta/b)$

are the same.

2.1.1 Launching

Part of the appeal of the MPS pulse is that a two-dimensional array launching scheme has already been proposed (Ziolkowski, 1989) and implemented (Ziolkowski and Lewis, 1990). Through use of Huygen's representation, a scalar field, such as the MPS pulse, can be defined at an observation point $\vec{r}$ within a closed surface as (Jones, 1964):

$$\begin{aligned} f(\vec{r},t) &= \int_{\mathcal{S}} \left[g(\vec{r},\vec{r'}) \left.\frac{\partial f}{\partial n'}\right|_{(\vec{r'},t-\frac{R}{c})} + \frac{1}{c}\left.\frac{\partial f}{\partial t}\right|_{(\vec{r'},t-\frac{R}{c})} g(\vec{r},\vec{r'})\frac{\partial R}{\partial n'} \right. \\ &\quad \left. - f\left(\vec{r'},t-\frac{R}{c}\right)\frac{\partial}{\partial n'}g(\vec{r},\vec{r'})\right] d\vec{s'} \end{aligned} \tag{2.12}$$

where n' is the inward pointing normal to the surface, $\mathcal{S}$, $\vec{r'}$ represents the source coordinates on $\mathcal{S}$, and R is the distance from the observation point to the source coordinates, $R = |\vec{r} - \vec{r'}|$. The function $g(\vec{r},\vec{r'})$ is the propagator $1/4\pi R$. So, the value of the function $f(\vec{r},t)$ can be determined at any point within the surface as long as the function and its derivatives are known over all points of the surface.

Consider the surface to be a hemisphere connected to an $x'y'$ plane centered at z', with the radius of the hemisphere $\rightarrow \infty$. In this case, every observation point with $z > z'$ is contained within the surface. Assuming no contribution from the hemisphere, the integral over the surface becomes a double integral over the $x'y'$ plane, with inward pointing normal $-\hat{z'}$. If the driving functions on the $x'y'$ plane are defined as:

$$\Psi\left(\vec{r'},t-\frac{R}{c}\right) = \left.\frac{\partial f}{\partial z'}\right|_{(\vec{r'},t-\frac{R}{c})} - \frac{z-z'}{R}\left.\frac{\partial f}{\partial ct}\right|_{(\vec{r'},t-\frac{R}{c})} - \frac{z-z'}{R^2} f\left(\vec{r'},t-\frac{R}{c}\right) \tag{2.13}$$

then the function can be expressed as:

$$f(\vec{r},t) = -\int_{-\infty}^{\infty}\int_{-\infty}^{\infty} \Psi\left(\vec{r'},t-\frac{R}{c}\right)\frac{1}{4\pi R}dx'dy' \tag{2.14}$$

Unfortunately, a continuous source over an infinite plane is not feasible so some approximations must be made. In Ziolkowski's proposed launching scheme (Ziolkowski, 1989), the integral is expressed as a summation over an $(2N+1) \times (2M+1)$ array of transducers as:

$$f(\vec{r},t) = -\sum_{n=-N}^{N}\sum_{m=-M}^{M} \Psi\left(n\Delta x, m\Delta y, z', t - \frac{R_{nm}}{c}\right)\Delta x \Delta y \frac{1}{4\pi R_{nm}} \tag{2.15}$$

where Δx and Δy are the element spacings in the x' and y' directions, and $R_{nm} = [(x - n\Delta x)^2 + (y - m\Delta y)^2 + (z - z')^2]^{1/2}$.

The array of transducers is both finite and discrete, so errors due to truncation and discretization are inevitable. The errors manifest themselves as a decrease in smoothness of the pulse and a decrease in the distance to which the pulse can be reconstructed, as will be demonstrated in Section 3.1.1.

Efforts have been made to minimize errors due to truncation and sampling while still maintaining a realistic array. One way to make a small array (radius r_{max}) act like a larger array is to 'fold' exterior points ($\rho' > r_{max}$) onto interior points using the conformal map $\rho' \mapsto r_{max}^2/\rho'$ (Ziolkowski, 1989).

For the planar array considered previously, all points $x'^2 + y'^2 > r_{max}^2$ will be mapped so that $x' \mapsto [r_{max}^2/(x'^2 + y'^2)]x' = \zeta$ and $y' \mapsto [r_{max}^2/(x'^2 + y'^2)]y' = \eta$. The Huygen's representation then becomes:

$$\begin{aligned} f(\vec{r},t) &= -\int_{-\infty}^{\infty}\int_{-\infty}^{\infty} \Psi\left(x', y', z', t - \frac{R}{c}\right)\frac{1}{4\pi R}dx'dy' \\ &= -\int_{-x_{max}}^{x_{max}}\int_{-y_{max}}^{y_{max}} \Psi\left(x', y', z', t - \frac{R}{c}\right)\frac{1}{4\pi R}dx'dy' \\ &\quad -\int_{-x_{max}}^{x_{max}}\int_{-y_{max}}^{y_{max}} \left(\frac{r_{max}^2}{\zeta^2 + \eta^2}\right)^2 \Psi\left(\zeta_f, \eta_f, z', t - \frac{R_f}{c}\right)\frac{1}{4\pi R_f}d\eta d\zeta \end{aligned} \tag{2.16}$$

where $\zeta_f = \zeta[r_{max}^2/(\zeta^2 + \eta^2)]$, $\eta_f = \eta[r_{max}^2/(\zeta^2 + \eta^2)]$, and $R_f = [(x - \zeta_f)^2 + (y - \eta_f)^2 + (z - z')^2]^{1/2}$.

Because the propagator term $(1/4\pi R)$ has the folded value for the distance from the source to the reconstruction point, R_f, rather than the actual distance from the transducer to the point, R, this is still an infinite array representation. To overcome this, Ziolkowski approximates the distance R_f by R, and introduces the appropriate time offsets for the retarded time in the folded term driving functions. The array now acts as a larger array, however the signals required by the sources are much more complicated. The folded portion is responsible for recreating the pulse at great distances from the array, while the non-folded term causes the reconstruction close to the array.

A potential problem arises in that the driving functions, $\Psi(\vec{r}', t - R/c)$, contain R and z in the multiplicative terms $(z - z')/R$ and $(z - z')/R^2$, which implies that the pulse can only be created at one point. This problem can be overcome with some assumptions. If the reconstruction point is relatively far from the generating array, relatively large compared to the size of the array, and close to the $z-$axis, then $(z - z') \approx R$ and $1/R \rightarrow 0$. In this case, the driving functions can be approximated by $\Psi \approx 2\partial_{ct} f$ (Ziolkowski, 1991), or equally well by $\Psi \approx 2\partial_{z'} f$.

Experiments have been conducted to verify the production of localized waves, and comparisons have been made with conventional continuous waves (Ziolkowski et al., 1989; Ziolkowski and Lewis, 1990). They have concluded that, using a two-dimensional array, localized waves can be launched which outperform their conventional counterparts in both beam quality and energy efficiency.

2.2 Ultrasound

Ultrasound[1] is widely used for non-invasive imaging of soft tissue. Over the past few years, the medical applications for this imaging modality have grown considerably. Reasons for

[1] Most of the information about ultrasound beams and imaging presented in this section is taken from *Ultrasound Physics and Instrumentation*, (Hykes et al., 1992)

this growth include the apparent harmlessness of ultrasound as well as advances in real-time instrumentation. So far, use of ultrasound has mainly been qualitative. Quantitative analysis capabilities would significantly enhance the diagnostic uses of the instrument.

The ideal ultrasonic beam would be unidirectional, uniform in intensity, and of limited dimensions for good spatial resolution. Both lateral and axial resolution are important, so the beam should be localized in both directions. Diffractive spreading is a serious problem with ultrasonic waves because the beams diverge at an angle proportional to their wavelength, and ultrasonic waves have a relatively large wavelength. It is the limiting factor in determining the resolution limits of this imaging modality.

It is possible to improve resolution through use of focusing techniques. Both mechanical and electronic methods of focusing are used. An acoustic lens or acoustic mirror can be used to mechanically focus the lens, however the most common technique of mechanical focusing for frequencies less than five MHz is to use a curved transducer crystal. Electronic focusing is accomplished by superimposing ultrasound waves from linear or matrix arrays of transducers. The signal from each transducer in the array is offset by an appropriate time delay so that the generated wave front arrives at a specific point at the same time, in phase. The result of this is a focused beam at that point.

Unfortunately, these methods of focusing have a very limited depth of field. To compensate for this, dynamic focusing and multiple pulses which are focused at different depths are employed. This, in turn, leads to low frame rates and unclear images for moving objects.

There are problems associated with using arrays of transducers and electronic focusing. Secondary lobes of ultrasonic energy are formed which cause artifacts to appear in the image. These lobes come in two varieties, side and grating. Side lobes are present with all transducers, but are reduced when the density of similar elements is increased. Grating lobes present a larger problem. They are caused by the regular, periodic spacing

of elements in the array and are especially prominent at strong interfaces.

Beams which have an extended depth of field, that is they will propagate without diffracting thereby not suffering loss of resolution, would be ideal for ultrasonic imaging. Both the FWM and MPS pulse fall into this category. Reduced resolution due to diffractive spreading is no longer an issue, and they don't suffer from limited depth of field or low frame rates like mechanically or electronically focused continuous waves. On the downside, the dense, independently addressable element arrays required to launch these waves could cause an increase in equipment cost.

Over the past few years, some emphasis has been placed on developing two dimensional arrays in order to improve further the diagnostic capabilities of ultrasound imaging. (Goldberg et al., 1992; Smith and Light, 1992). These arrays are being developed to improve launching and reception of continuous waves, however it is possible that they could be configured to launch localized waves.

Chapter 3

Localized Wave Performance

This chapter contains a study of the characteristics and limitations of localized waves generated from a finite, discrete array of transducers. The study is conducted through computer simulations of the array launching procedure proposed by Ziolkowski, (Ziolkowski, 1989), described in Section 2.1.1. The effects of array size and element spacing will be explored, along with the use of folding to expand an array. The possibility of generating a FWM pulse is considered, and the FWM is compared to the MPS pulse. Finally, research into development of two-dimensional arrays will be considered in order to decide what array dimensions may be considered for realistic application to launching localized ultrasound waves.

3.1 Launching Localized Waves: The MPS Pulse

For the purposes of illustration, dimensionless coordinates will be introduced, along with the characteristic variables $u = z - ct$ and $v = z + ct$. To non-dimensionalize the variables in the equation describing the MPS pulse, (2.10), they will be multiplied by b/β. The new coordinates will be $(\rho_1, u_1, v_1) = b/\beta(\rho, z - ct, z + ct)$ where, as before, $\rho^2 = x^2 + y^2$. Using these coordinates, along with the new parameters $z_0' = bz_0/\beta$ and $a_1 = ab$, and assigning $\alpha = 1$, the form of the MPS pulse is:

$$f(\rho_1, u_1, v_1) = \frac{b^2}{\beta} \frac{1}{z_0' + iu_1} \frac{1}{s_1 + a_1} e^{-s_1} = \frac{b^2}{\beta} f_1(\rho_1, u_1, v_1) \tag{3.17}$$

where

$$s_1 = s_1(\rho_1, u_1, v_1) = \frac{\rho_1^2}{z_0' + iu_1} - iv_1 \tag{3.18}$$

The source functions for the following simulations will use the approximation $\Psi \approx 2\partial_{z'} f$, as the results are virtually identical to those when the full function (Equation (2.13)) is used. Using the dimensionless coordinates and parameters, and ignoring the multiplicative constant because it can be adjusted later, the source functions are:

$$S(\rho_1', u_1' + R_1, v_1' - R_1) = \left.\frac{\partial f_1}{\partial u_1'}\right|_{(\rho_1', u_1' + R_1, v_1' - R_1)} + \left.\frac{\partial f_1}{\partial v_1'}\right|_{(\rho_1', u_1' + R_1, v_1' - R_1)} \tag{3.19}$$

where

$$\frac{\partial f_1}{\partial u_1'} + \frac{\partial f_1}{\partial v_1'} = \left[\frac{-i}{z_0' + iu_1'} - \left(\frac{1}{s_1 + a_1} + 1\right)\left(\frac{\partial s_1}{\partial u_1'} + \frac{\partial s_1}{\partial v_1'}\right)\right] f_1 \tag{3.20}$$

and

$$\frac{\partial s_1}{\partial u_1'} + \frac{\partial s_1}{\partial v_1'} = -i\left[\frac{\rho_1'^2}{(z_0' + iu_1')^2} + 1\right] \tag{3.21}$$

R_1 is the distance from the source to the reconstruction point. For an array of N transducers, the reconstructed value of the function f_1 is:

$$f_1(\rho_1, u_1, v_1) = -\sum_{n=1}^{n=N} S(\rho_{1_n}', u_1' + R_1, v_1' - R_1)\frac{1}{4\pi R_{1_n}} dA_n \tag{3.22}$$

where ρ_{1_n}' is the distance from the origin to the n^{th} source in the source plane, and dA_n is the area represented by that source. For an evenly spaced square array, $dA_n = \Delta x_1 \Delta y_1$, where Δx_1 and Δy_1 are the element spacings in the x_1' and y_1' directions.

For the simulations that follow, the summation over the sources given by Equation (3.22) was calculated using original C code. The real part of the reconstructed wave is displayed using Xmath software.

3.1.1 Array Considerations

There are many considerations when deciding upon an optimal array, such as the shape of the array, size, element spacing, and whether to utilize the folded array scheme. Of

these factors, array shape is probably the least important. Although it makes sense to use a circular array in that the magnitudes of the driving functions decrease radially from the origin, it is easier to construct and manipulate an evenly spaced square array. It seems that the arrays that are actually being developed are of the square or rectangular variety (Smith and Light, 1992), so that is what will be used here. The rest of the factors deserve further, in depth consideration and will be discussed in the following sections.

Array Size and Element Spacing

Array size and element spacing both greatly affect the quality of the reconstructed pulse. Element spacing seems to have its greatest effect on the smoothness of the reconstructed pulse, especially in the trailing wake. Array size determines the distance to which the pulse can be reconstructed. These effects are demonstrated in Figure 3.4 for the MPS pulse at $v_1 = 2\pi$ with parameters $a_1 = 600$ and $z_0' = 9.0 \times 10^{-4}$. The first waveform, Figure 3.4a, is the MPS pulse. Next, Figure 3.4b, is the MPS pulse as reconstructed from a 21×21 square array, with element spacing $\Delta x_1' = \Delta y_1' = 0.02$. The next reconstruction, Figure 3.4c, is from a 21×21 square array which is made twice as large by doubling the element spacing to $\Delta x_1' = \Delta y_1' = 0.04$. The reconstruction appears to be more accurate, in that the fundamental shape of the pulse is more like that of Figure 3.4b. The larger array has produced the leading wake which was missing in the reconstruction from the smaller array. The courser element spacing, however, has increased the choppiness in the trailing wake. Finally, Figure 3.4d is a reconstruction from an array which was doubled in size (compared to Figure 3.4b) by increasing the number of elements to 41×41 and leaving the spacing at $\Delta x_1' = \Delta y_1' = 0.02$. In this pulse, the reconstruction error caused by the course spacing has been smoothed significantly. In all cases, the pulses have been normalized to their maximum values at $\rho_1 = 0$ and $u_1 = 0$.

The above discussion is of a qualitative nature, and while it can be used to get an

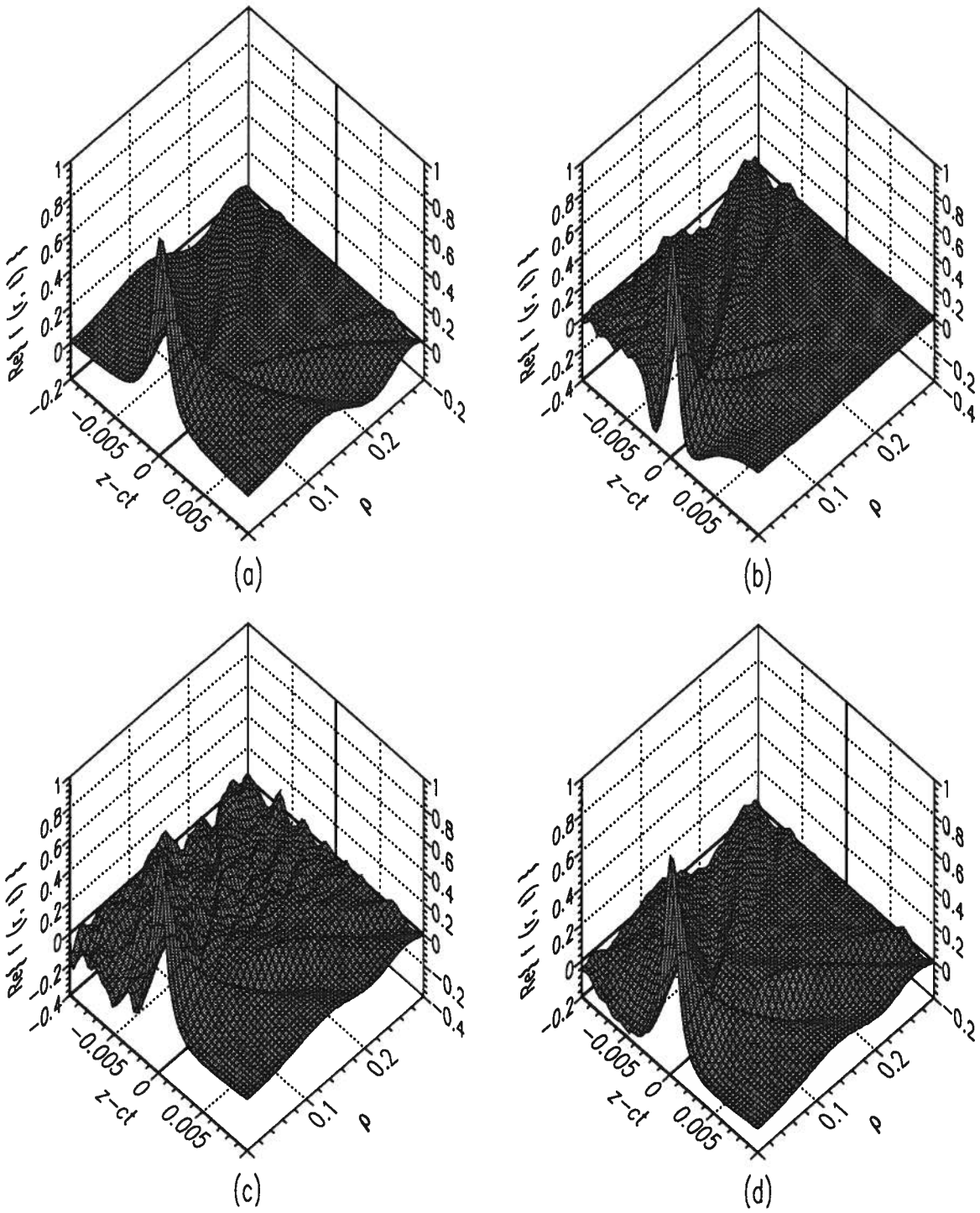

Figure 3.4: The MPS pulse and reconstructions for parameters $a_1 = 600$ and $z_0' = 9.0 \times 10^{-4}$; a) the MPS pulse at $v_1 = 2\pi$; b) reconstruction from a 21×21 array with spacing $\Delta x_1' = \Delta y_1' = 0.02$; c) reconstruction from a 21×21 array with spacing $\Delta x_1' = \Delta y_1' = 0.04$; and d) reconstruction from a 41×41 array with spacing $\Delta x_1' = \Delta y_1' = 0.02$.

idea as the effects of array size and element spacing, a quantitative description of these effects would be more informative. Following is an attempt to separate and quantify the effects of these two factors.

Array Size The maximum distance to which the pulse can be reconstructed is completely determined by array size. This can be seen through examination of either the driving functions for different values of v_1, which is representative of twice the reconstruction distance, or the reconstruction at the pulse center for different array sizes as a function of v_1. The driving functions will be investigated first.

Since the driving functions are circularly symmetric, any line through the origin is representative of their evolution. For $u_1 = 0$ and varying values of v_1, the required source function, as given in Equation (3.19) is charted as a function of ρ_1'. As v_1 is increased, the distance from the origin at which there are significant contributions also increases. The increase in required array size varies approximately linearly with reconstruction distance, as illustrated in Figure 3.5. Figure 3.5a is the source function for $v_1 = 2\pi$ and Figure 3.5b is for $v_1 = 20\pi$. The value of ρ_1' to which the driving function has significant amplitude is approximately ten times greater for the reconstruction at $v_1 = 20\pi$ than for $v_1 = 2\pi$. The values of the other parameters are $a_1 = 600$ and $z_0' = 9 \times 10^{-4}$.

Reinforcing the observation that array size determines reconstruction distance is the investigation of the reconstruction at the pulse center as a function of array size. As the array size increases, the distance to which the pulse can be reconstructed also increases. The evolution of the pulse at the pulse center is the same for a given array size, regardless of the number of elements in the array, as illustrated in Figures 3.6 and 3.7. Figure 3.6 shows the evolution of the reconstructed pulse at the pulse center ($u_1 = 0$, $\rho_1 = 0$) as a function of v_1 for three different arrays, all of the same size but with different numbers of elements. The total array size is 1.6×1.6 for all three cases, but in the first, the

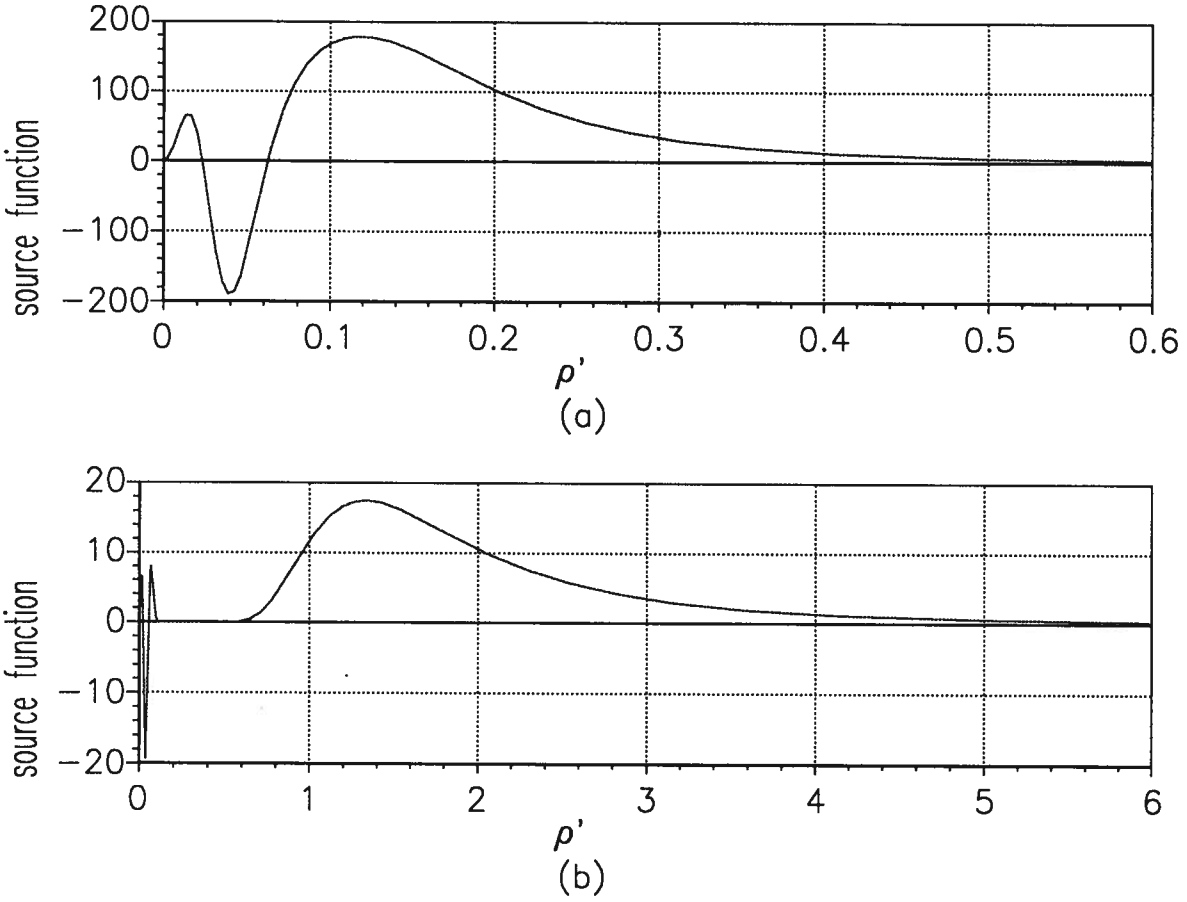

Figure 3.5: The driving functions as a function of ρ_1' for (a) $v_1 = 2\pi$ and (b) $v_1 = 20\pi$

array is 21×21 elements with element spacing 0.08, the second is from a 41×41 array with element spacing 0.04, and the third features an 81×81 array with element spacing 0.02. The distance to which the pulse can be reconstructed does not improve with the increase in source elements and accompanying decrease in element spacing. Figure 3.7 shows the evolution of the reconstructed pulse at the pulse center as a function of v_1 for arrays which are ten times the size of those in Figure 3.6. The first plot is from a 21×21, array with element spacing 0.80, next is from a 41×41 array with element spacing 0.40, and the third demonstrates the reconstruction due to an 81×81 array with element spacing 0.20. As before, the number of elements, and therefore element spacing, does

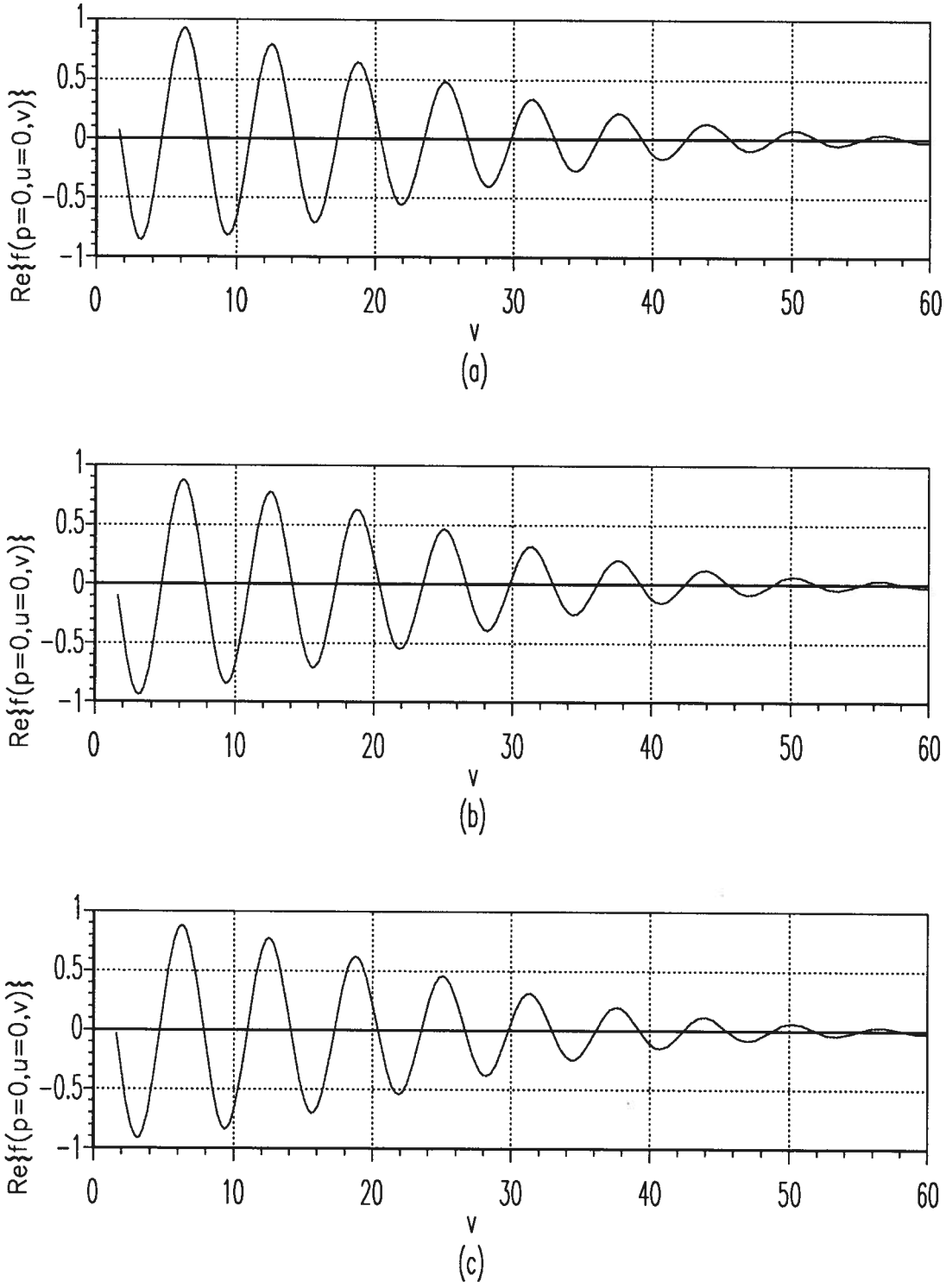

Figure 3.6: Evolution of reconstructed pulse at the pulse center as a function of v_1 for an array of size 1.6×1.6 with a) 21×21, b) 41×41, and c) 81×81 elements.

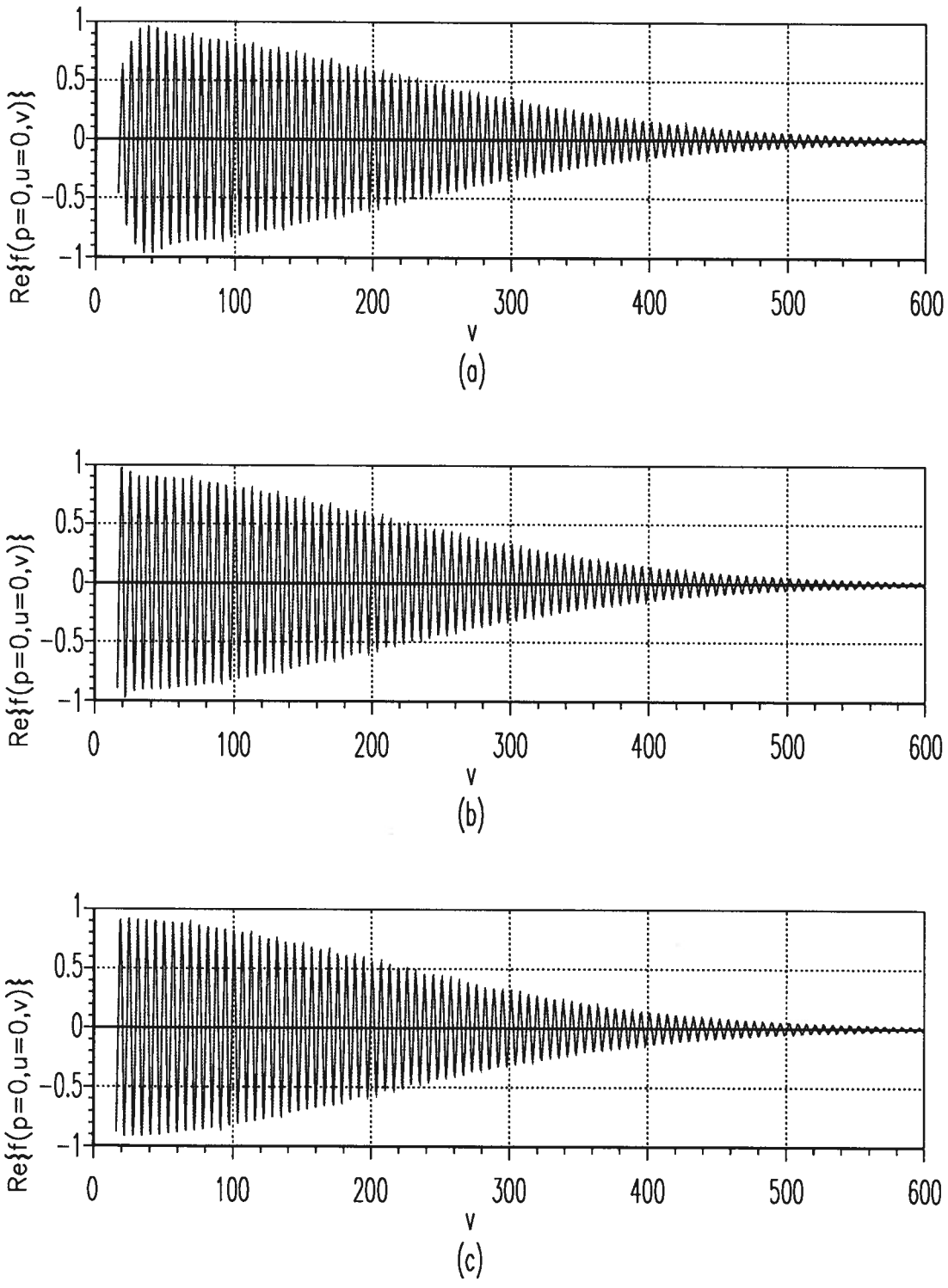

Figure 3.7: Evolution of reconstructed pulse at the pulse center as a function of v_1 for an array of size 16×16 with a) 21×21, b) 41×41, and c) 81×81 elements.

not affect the maximum reconstruction distance. However, in this case, the propagation distance before the decay behavior is observed is approximately ten times that for the arrays which are ten times smaller. As before, the values of the other parameters are $a_1 = 600$ and $z_0' = 9 \times 10^{-4}$.

Element Spacing Analysis of the driving functions, as a function of ρ_1' for different values of reconstruction distance, v_1, also yields information about the effects of element spacing. Through application of a Fourier transform, the spectrum of a function can be found. If the transform is approximately zero for frequencies greater than a cut-off frequency, f_c, then the function is bandlimited. If a bandlimited function is sampled at intervals less than or equal to $1/2f_c$, it can be accurately reconstructed from the samples. Sampling at larger intervals results in aliasing, which degrades the reconstruction. So, the required array element spacing can be determined by taking the spatial Fourier transform of the driving functions. To investigate this, the evolution of the required source function, given in Equation (3.19), as a function of x_1', with $y_1' = 0$, was used. The spatial Fourier transform of the source function was found numerically for different values of v_1. The resulting spectra for $v_1 = 2\pi$ and $v_1 = 20\pi$ are illustrated in Figure 3.8. In the figure, the transforms are normalized to their maximum values. Although increasing the reconstruction distance increases the distance from the origin at which there are significant contributions by the driving functions, the spectrum remains mostly unchanged. If a cut-off frequency is defined as the frequency after which the spectrum does not rise to above one per cent of it's maximum value, then the cut-off frequency for both values of v_1 are similar. For $v_1 = 2\pi$, the cut-off frequency is around 35, while for $v_1 = 20\pi$ it is about 25. There is a slight decrease, but both are of the same order of magnitude. This means that the spacing required to produce a good reconstruction does not change. In short, to increase the distance to which the pulse can be reconstructed, the array needs to

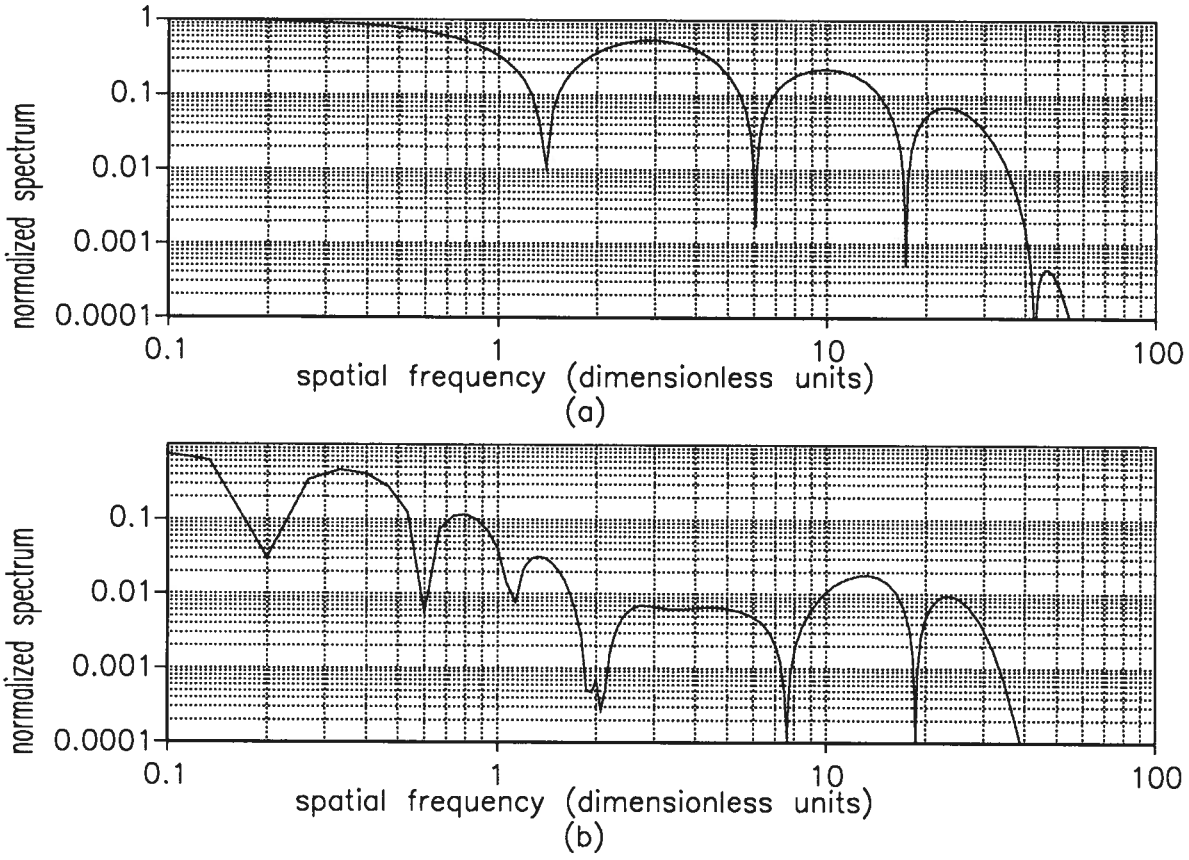

Figure 3.8: Normalized spectra of driving functions for $v_1 = 2\pi$ and $v_1 = 20\pi$.

be made larger. To accomplish this, the number of elements should be increased rather than simply increasing the element spacing.

The Folded Array Configuration

Whether or not to use the folded array configuration is another important consideration. The driving functions for the folded array can produce a reconstructed pulse at further distances from the generating array, but they are much more complicated and are of greater amplitude than the non-folded driving functions. These factors may be important in terms of transducer limitations.

For comparison purposes, reconstructions using both the regular and the folded source functions from the same array were simulated. The value of the reconstructed pulse as a function of propagation distance is compared, as well as the driving functions required.

The source functions used to drive the elements in the folded array configuration consist of the regular, non-folded term (S, as given in Equation (3.19)) along with a second term representing the folded elements. For an array in which the farthest element from the origin is at $\rho_1' = r_{max}$, folded coordinates can be defined as $x_{1_f}' = x_1'[r_{max}^2/\rho_1'^2]$ and $y_{1_f}' = y_1'[r_{max}^2/\rho_1'^2]$. Using these folded coordinates, the folded portion of the source functions is:

$$S_f = \left(\frac{r_{max}^4}{\rho_1'^4}\right) S(x_{1_f}', y_{1_f}', u_1' + R_f, v_1' - R_f) \tag{3.23}$$

where $R_f = [(x_1 - x_{1_f}')^2 + (y_1 - y_{1_f}')^2 + (z_1 - z_1')^2]^{1/2}$ is the distance from the folded coordinates to the reconstruction point. Adding this folded term to the non-folded term makes the source element at (x_1', y_1', z_1') behave like it is also at $(x_{1_f}', y_{1_f}', z_1')$. When the folded term is incorporated into the summation formulation for the value of the reconstructed function, Equation (3.22), the value for R used in the propagator $(1/4\pi R)$ is R_1 rather than R_f, since the distance to the reconstruction point is really R_1. The function, then, is given by:

$$f_1(\rho_1, u_1, v_1) = -\sum_{n=1}^{n=N} (S + S_f)\frac{1}{4\pi R_{1_n}} dA_n \tag{3.24}$$

Figure 3.9 shows the evolution of the reconstructed MPS pulse at the pulse center as a function of v_1 for source functions both with and without the folded term. The generating array in both cases has 21×21 elements with element spacing 0.01, making the array size 0.2×0.2. The values of the other parameters are $a_1 = 600$ and $z_0' = 9 \times 10^{-4}$, as in the preceding sections. When very close to the array, the two reconstructions are indistinguishable, but the pulse generated without the folded term decays quickly, while the pulse generated by the folded array appears to propagate at least an order of

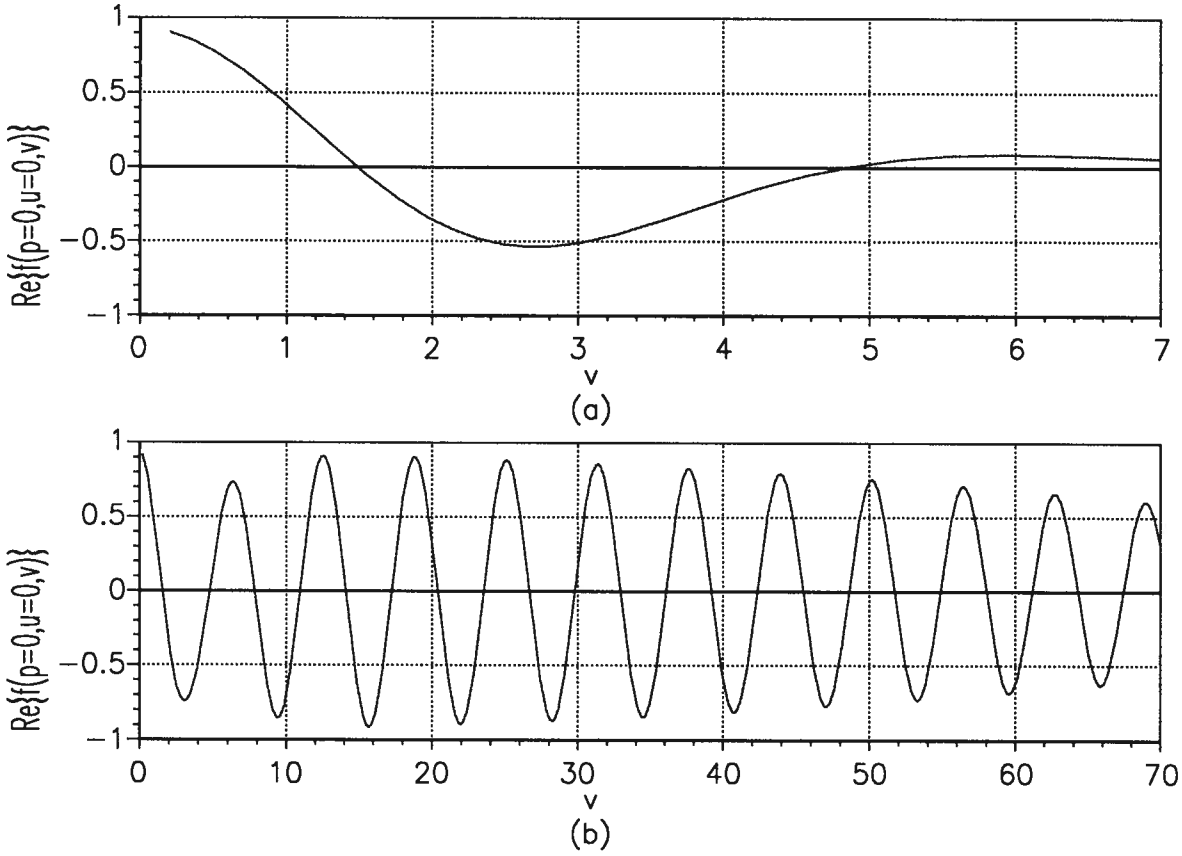

Figure 3.9: Evolution of the reconstructed MPS pulse as a function of v_1 from a 21×21 element array of size 0.2×0.2 for source functions (a) without and (b) with the folded term.

magnitude farther, experiencing only a slight drop where the non-folded pulse decays before recovering. This drop is probably because the folding is intended for a round array, so when incorporated for a square array that fits inside the corresponding round array, there are gaps that will be most noticeable at the point where the folded term first starts to dominate.

The graph depicting the evolution at the pulse center for the folded array looks encouraging, but this may be deceiving. The reconstruction error due to element spacing must be considered as well. The effective spacing for the folded elements increases as the

square of the distance from the origin to the represented point. So, the effective element spacing becomes very course for the distant folded elements. Since these elements are responsible for recreating the pulse at greater distances from the array, it is worthwhile to examine the actual pulse reconstructions for some different values of the reconstruction distance that are due to the folded term.

Figure 3.10 shows the reconstructed pulse at distances of $v_1 = 2\pi$, 6π, 10π, and 20π for the same pulse as in the preceding figure. Comparing these reconstruction distances to the plot of the evolution of pulse center, Figure 3.9, shows that at $v_1 = 2\pi$, the folded term is starting to dominate, while for the greater distances the reconstruction is due entirely to the folded term. At $v_1 = 2\pi$, the reconstruction is not bad, with the pulse being easily distinguishable from the surrounding noise, but it deteriorates as the distance increases, with the pulse being virtually indistinguishable from the reconstruction error at $v_1 = 20\pi$. This deterioration is due to the increased effective spacing. So, although the pulse has not yet decayed to half its maximum value, the quality of the reconstructed pulse is such that it is of not much use. This means that although the folded source functions can produce a pulse to a greater distance, this distance is not nearly as great as the evolution at the pulse center seems to promise.

While application of the folded source functions can generate a reconstructed pulse at greater distances from the array, there is a cost involved. Figure 3.11 shows the time (actually $(b/\beta)ct$) evolution of the source function required of a transducer located at a distance of $\rho_1' = 0.04$ from the origin in the source plane, for an array of size 0.2×0.2. The source function is divided into the non-folded and folded terms. The folded term is much more complicated than the non-folded component, and three orders of magnitude larger. Also, the folded term grows increasingly more complicated as the element involved approaches the center of the array. The driving function considered in the figure is close to the center, but for an array with the element spacing considered earlier, it is not the

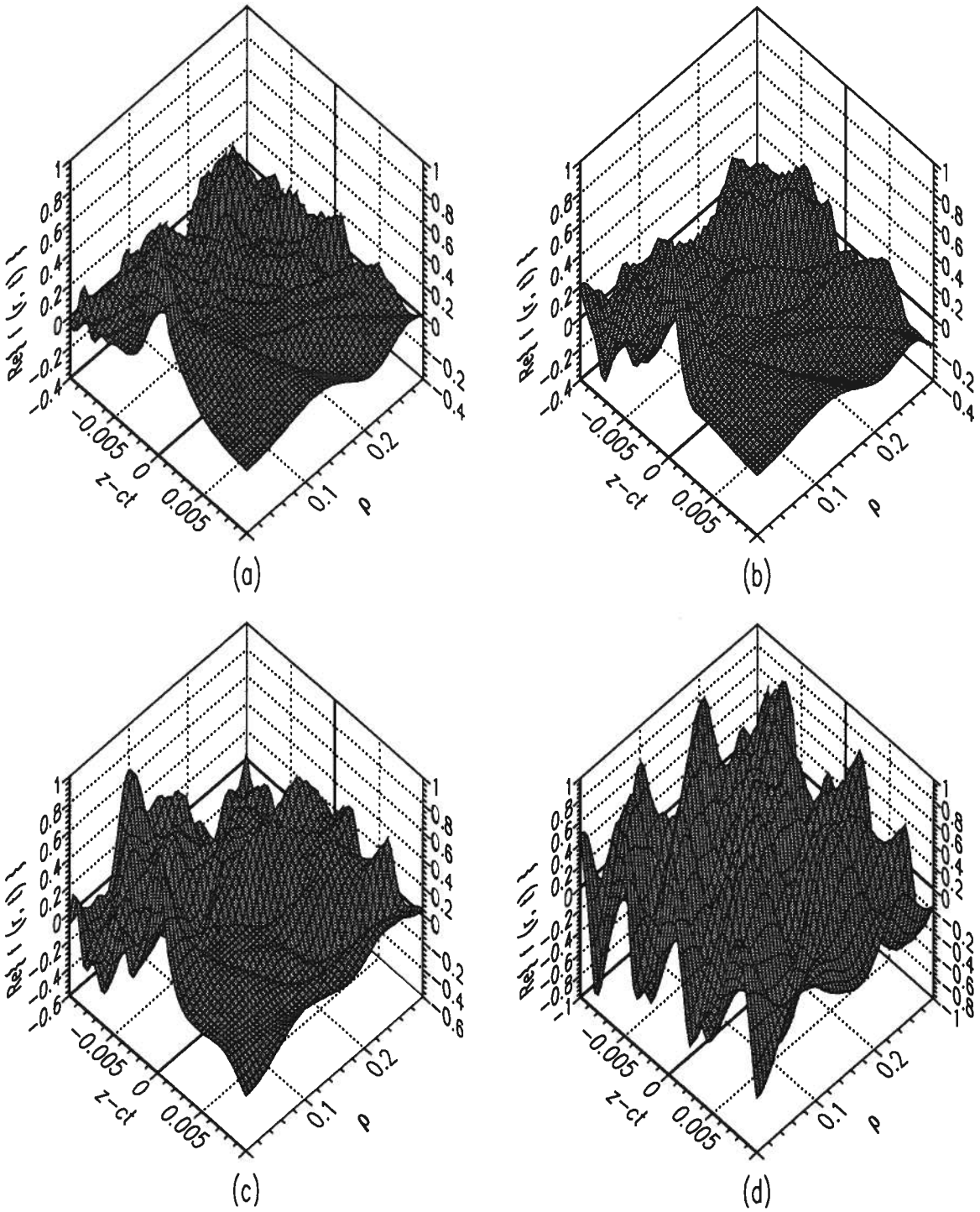

Figure 3.10: The MPS pulse as reconstructed from a 21×21 element array of size 0.2×0.2 using the folded source functions at distances of $v_1 = 2\pi$, 6π, 10π, and 20π.

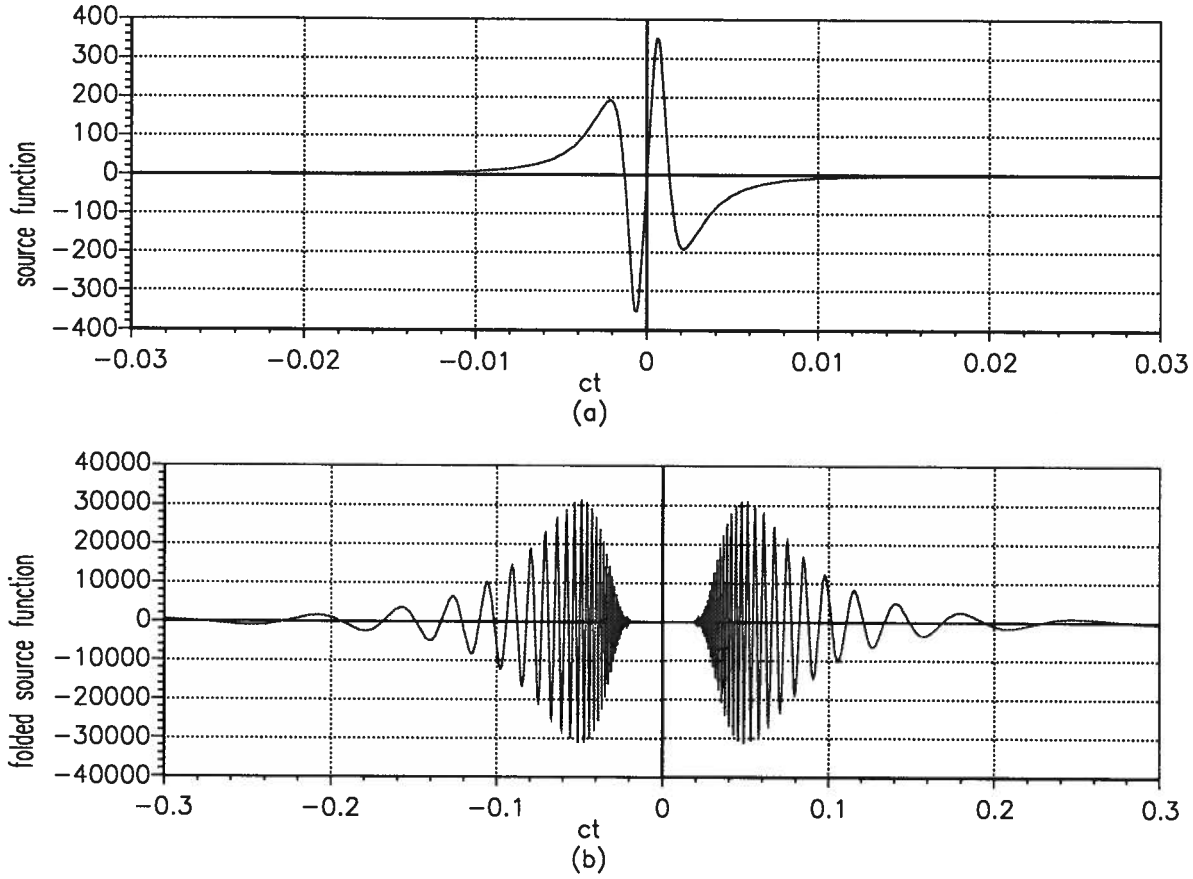

Figure 3.11: The time evolution of the non-folded (top) and folded (bottom) terms of the driving function at $\rho_1' = 0.04$ in an array of size 0.2×0.2.

closest, therefore not the most complicated.

3.2 The Focus Wave Mode

The expected propagation characteristics for the MPS pulse are never achieved in a reconstruction from a finite array. For $v_1 < a_1$, the pulse is supposed to oscillate but not decay, which does not occur. Rather, as is apparent in Figures 3.6 and 3.7, the height of the pulse at the pulse center starts to decay almost immediately. This leads to a couple of points which require further investigation.

The first point is that although the source functions used to drive the array determine the pulse shape, it seems that the array actually determines the propagation distance. It was previously thought that in order for a pulse to be launched, it had to be of finite energy. For this reason, the MPS pulse was introduced, rather than trying to launch the original FWM. The MPS pulse has a term which causes the pulse to decay as $1/v_1$ in the region $v_1 \geq a_1$, whereas if the FWM is charted, it never decays. If, however, the decay behavior caused by the array limitations overrides the natural propagation characteristics of the wave in question, there is no longer a problem. The fact that the pulse is launched from a finite array guarantees that it is of finite energy.

The difference between the waves can be seen most easily through examining the expressions for both pulses at their pulse centers, $\rho_1 = 0$ and $u_1 = 0$. The real part of the MPS pulse evolves as:

$$\Re\{f_1(\rho_1 = 0, u_1 = 0, v_1)\} = \frac{1}{a_1 z_0'} \frac{1}{1 + \frac{v_1^2}{a_1^2}} \left(\cos v_1 - \frac{v_1}{a_1} \sin v_1 \right) \tag{3.25}$$

while the real part of the FWM evolves as:

$$\Re\{\phi_1(\rho_1 = 0, u_1 = 0, v_1)\} = \frac{1}{z_0'} \cos v_1 \tag{3.26}$$

In the region where $v_1 < a_1$, the value of v_1/a_1 is insignificant, making the MPS evolution $\cos v_1/(a_1 z_0')$, which is the same as for the FWM. At great distances from the array, $v_1 > a_1$, the value of v_1/a_1 grows significant and the MPS pulses behavior becomes $\sin v_1/(z_0' v_1)$

The previous paragraph establishes the main difference between the two waveforms as the multiplicative term which causes the MPS pulse to decay as $1/v_1$ in the region $v_1 > a_1$. The fact that decay due to the finite size of the array occurs long before this region makes that term of limited importance. For this reason, it may be interesting to try to launch a FWM pulse using the same method as described for producing the MPS pulse, that

is, try driving an array of transducers using source functions $2\partial_{z_1'}\phi(\rho_1', u_1' + R, v_1' - R)$, where ϕ describes the FWM solution of the wave equation, as given in (2.5).

The second point is that the effect of the premature decay behavior on the localization of the pulse needs to be investigated. It is important to know if the decay is accompanied by spreading of the pulse. The decay is a problem, in that it decreases the strength of the signal, but spreading is a greater problem because it causes a decrease in resolution.

3.2.1 Launching FWM Pulses

The equation describing the FWM, (2.5), is non-dimensionalized by multiplying the variable by the parameter k. As with the MPS pulse earlier, the characteristic variables $u = z - ct$ and $v = z + ct$ will also be used. Using the variables $(\rho_1, u_1, v_1) = k(\rho, u, v)$ and the parameter $z_0' = kz_0$, Equation (2.5) is:

$$\phi(\rho_1, u_1, v_1) = \frac{k}{4\pi i}\frac{1}{z_0' + iu_1} e^{\frac{-\rho_1^2}{z_0' + iu_1}} e^{iv_1} = \frac{k}{4\pi i}\phi_1(\rho_1, u_1, v_1) \tag{3.27}$$

The same launching method and approximations to the driving functions as described for the MPS pulse will be used to create a FWM pulse. The source functions are:

$$S_{FWM}(\rho_1', u_1' + R_1, v_1' - R_1) = \left.\frac{\partial\phi_1}{\partial u_1'}\right|_{(\rho_1', u_1' + R_1, v_1' - R_1)} + \left.\frac{\partial\phi_1}{\partial v_1'}\right|_{(\rho_1', u_1' + R_1, v_1' - R_1)} \tag{3.28}$$

where

$$\frac{\partial\phi_1}{\partial u_1'} + \frac{\partial\phi_1}{\partial v_1'} = \left[\frac{i\rho_1'^2}{(z_0' + iu_1')^2} + i - \frac{i}{z_0' + iu_1'}\right]\phi(\rho_1', u_1', v_1') \tag{3.29}$$

These source functions are used to excite an array of transducers, as with the MPS pulse, thereby launching a FWM pulse.

To compare the FWM results with the MPS results, both pulses were simulated using the same value for the parameter z_0', arrays of the same size and number of elements, and at the same distances from the generating array. The results for both pulse types are remarkably similar, as will be demonstrated.

Comparison to MPS Pulse

When the evolution of the reconstructed FWM pulse at the pulse center is examined, it appears exactly the same as that for the MPS pulse. Figure 3.12 shows the evolution of both reconstructed pulses, normalized to their maximum values at $v_1 = 2\pi$, and the difference between them for a 41×41 element array with element spacing $\Delta = 0.04$. The reconstructed MPS, Figure 3.12b, is the same as that from Figure 3.6b. Both the FWM, Figure 3.12a, and the MPS pulse appear to decay at the same rate, which reinforces the opinion that it is actually the array that determines propagation distance. The difference between the two, Figure 3.12c, is two orders of magnitude smaller than the pulse height, so although it exists, it is not immediately evident.

Both pulses look the same when reconstructions in an area around the pulse center are examined. Figure 3.13 shows reconstructions of the FWM pulse at $v_1 = 2\pi$ and $v_1 = 4\pi$, Figures 3.13a and 3.13b, and reconstructions of the MPS pulse at the same distances, Figures 3.13c and 3.13d, for the same parameters and array given earlier. As in the case of the evolution at the pulse center, they look exactly the same. Small differences, two orders of magnitude smaller than the peak height, become apparent when the normalized pulses are subtracted, as shown in Figure 3.14. The waveforms in this figure result from subtracting the normalized MPS pulse from the normalized FWM pulse at $v_1 = 2\pi$, Figure 3.14a, and at $v_1 = 4\pi$, Figure 3.14b. At both distances, the difference between the two pulses is small, however it increases at the greater distance.

It is not surprising that the reconstructions of the two different pulses are so similar. Close to the array (for $v_1 < a_1$), they should both have the same behavior, as evidenced by Equations (3.25) and (3.26). It is only when the pulse has propagated a distance away from the array, so that the term which causes the decay in the MPS pulse $(1/(1+v_1^2/a_1^2))$ has some effect, that any differences are expected. The comparisons between the two

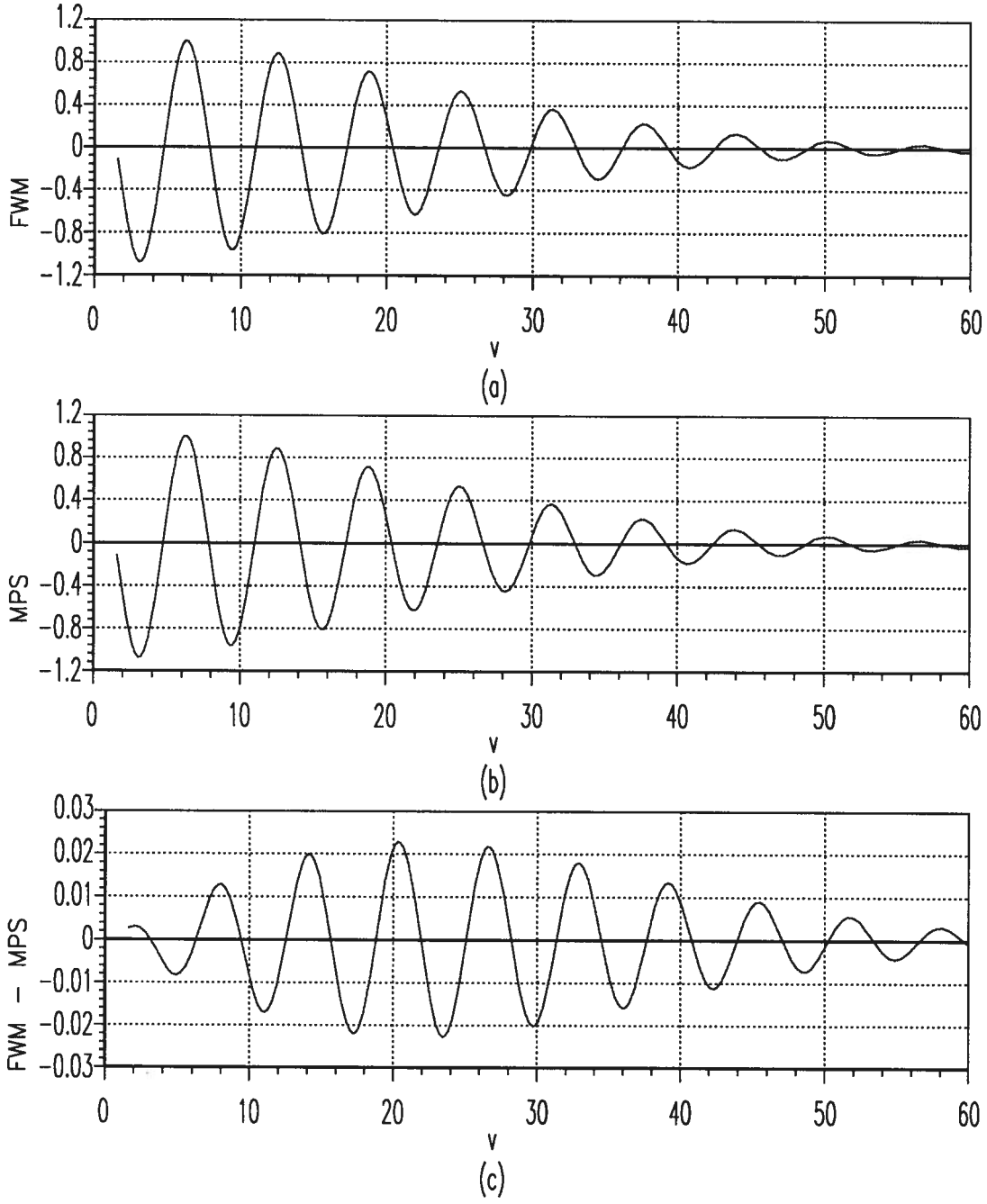

Figure 3.12: Evolution of reconstructed pulse at the pulse center as a function of v_1 for an array of size 1.6 with 41 $\times$ 41elements: a) the FWM; b) the MPS pulse; c) the difference between the two.

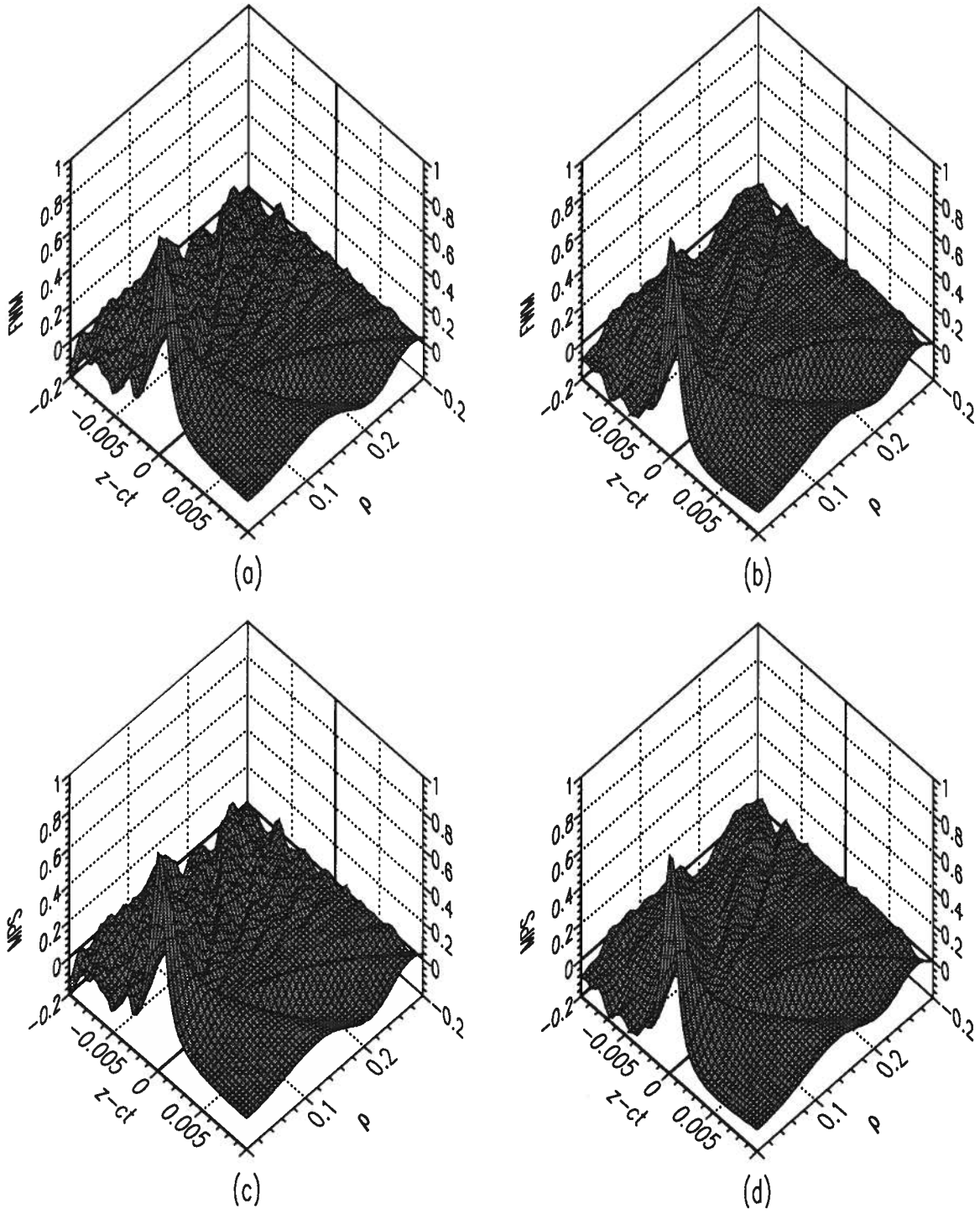

Figure 3.13: Reconstructions of the FWM at a) $v_1 = 2\pi$ and b) $v_1 = 4\pi$, and the MPS pulse at c) $v_1 = 2\pi$ and d) $v_1 = 4\pi$

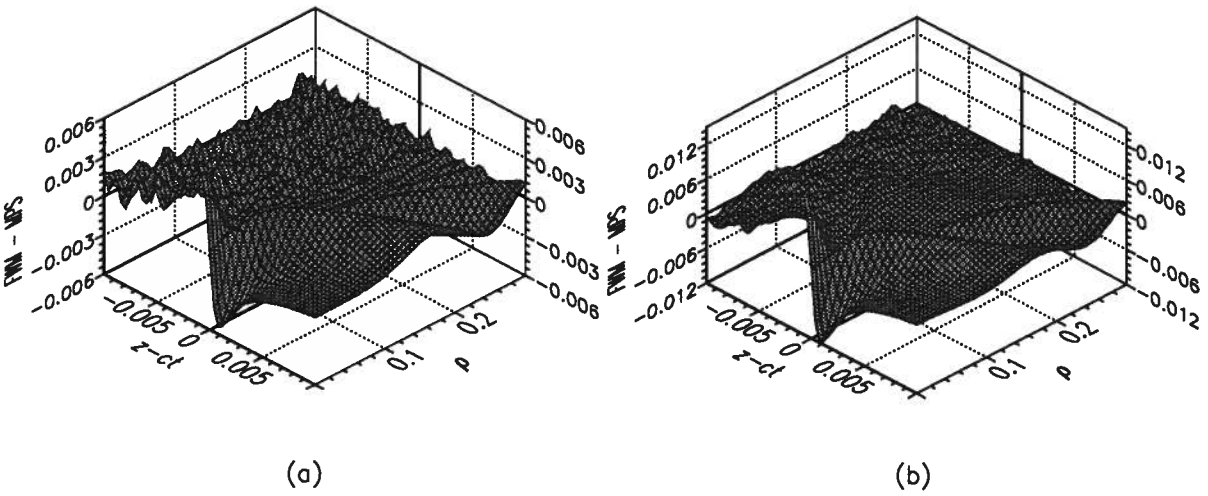

Figure 3.14: The difference between the normalized FWM and MPS pulse at a) $v_1 = 2\pi$ and b) $v_1 = 4\pi$

show that the slight differences between the two reconstructed pulses increase as the propagation distance, which is consistent with the expected behavior.

3.2.2 Pulse Behavior as it Decays

Now, the effects of the premature decay brought on by the array launching will be examined. A FWM pulse, reconstructed from an array of size 1.6 × 1.6 with 41 × 41 elements will be examined at distances of $v_1 = 2\pi, 4\pi, 6\pi$, and 8π. According to the graph showing the evolution at the pulse center as a function of v_1, Figure 3.12a, significant

decay occurs through this region. Figure 3.15 depicts the pulse shape as a function of u_1 at $\rho_1 = 0$ at these values of v_1, while Figure 3.16 shows the pulse as a function of ρ_1 at $u_1 = 0$. In all cases, the pulses have been normalized to their maximum values for ease of comparison.

The figures show that, although the array launching causes the pulse to decay before it is expected to, the decay is not immediately accompanied by spreading. The reconstruction error increases slightly, but the pulse is still easily distinguishable. Since the focused nature of the pulse is retained, the decrease in intensity of the pulse should cause no resolution problems.

3.3 Current Arrays

An important consideration when deciding upon an array to use is the dimensions which can realistically be attained.

Development of two-dimensional arrays has become an important part of ultrasound research. A 16×16 element transducer array with $0.6mm$ element spacing, expanded to a 16×16 array of connector pins at a standard spacing of $2.5mm$ has been reported (Smith and Light, 1992; Goldberg et al., 1992). This shows that very dense spacing is possible, and the value of $0.6mm$ will be used as a lower bound on element spacing. Since the presence of a transducer at the origin is important, in order to maintain a symmetric array 17×17 will be used as an upper bound on the number of array elements.

To summarize the results of this chapter, the size of the array determines the distance to which the pulse can be reconstructed, and the element spacing is responsible for the smoothness of the reconstruction. For course element spacing, there is reconstruction error which manifests itself in a roughness in the trailing wake. Although a larger array is required to generate a pulse at greater distances from the source, the required element

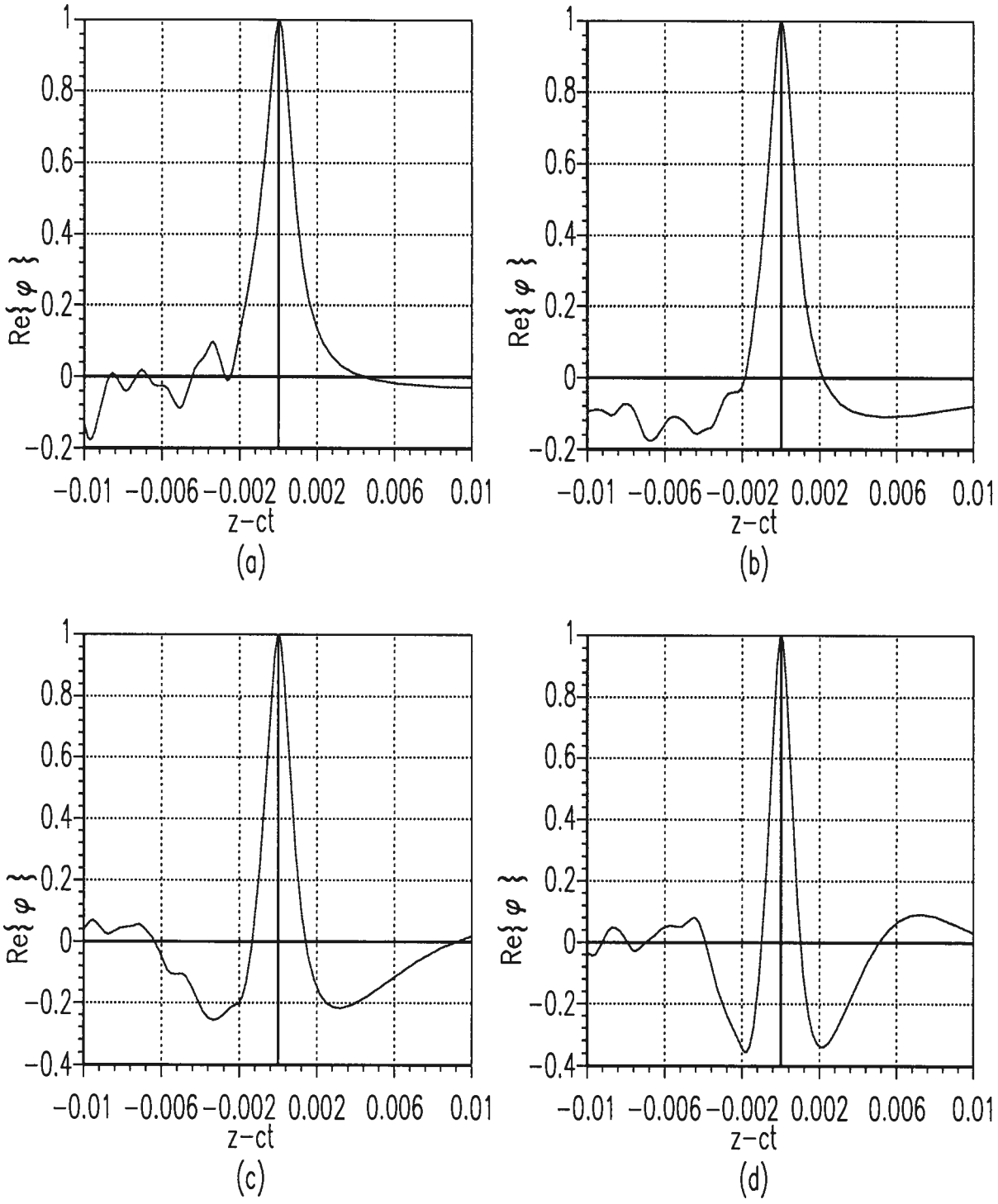

Figure 3.15: FWM normalized pulse as a function of u_1 at $\rho_1 = 0$ for pulse centers a) $v_1 = 2\pi$, b) $v_1 = 4\pi$, c) $v_1 = 6\pi$, and d) $v_1 = 8\pi$

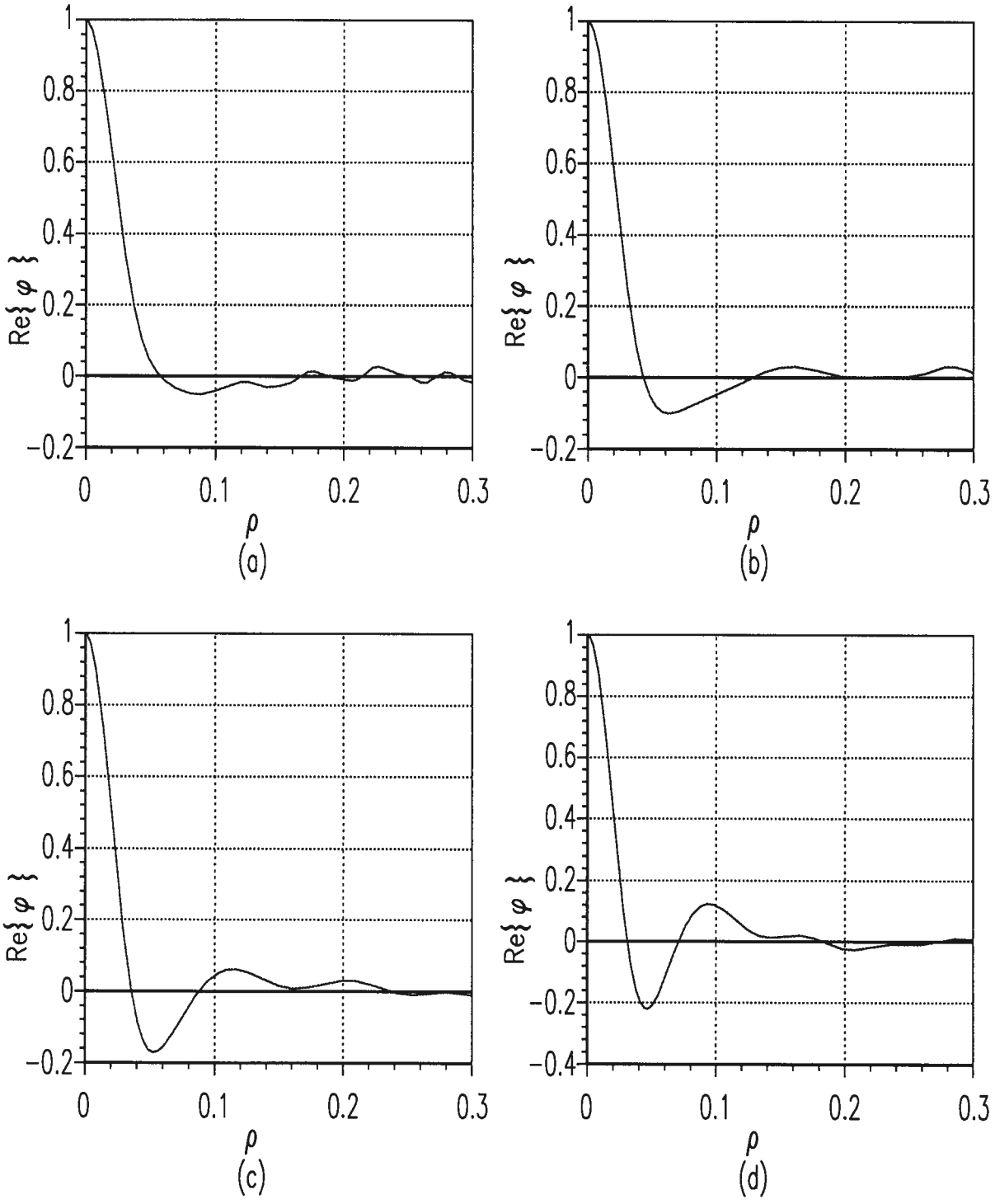

Figure 3.16: FWM normalized pulse as a function of ρ_1 at $u_1 = 0$ for pulse centers a) $v_1 = 2\pi$, b) $v_1 = 4\pi$, c) $v_1 = 6\pi$, and d) $v_1 = 8\pi$

spacing does not increase. This means that the array must be made larger by increasing the number of elements rather than increasing the distance between the elements.

The folded array configuration will cause the pulse to propagate farther than the non-folded, but not as far as anticipated while maintaining a smooth reconstruction. The effective course element spacing makes the pulse indistinguishable from reconstruction error after an unexpectedly short distance. The source functions are much more complicated, making the folded array configuration of little practical importance, since the gains are not worth the cost.

The array determines the propagation distance, overriding the expected propagation characteristics of either the MPS pulse or FWM. For this reason, the FWM can be reconstructed as effectively as the MPS pulse. When normalized reconstructions of each pulse are compared, the difference is two orders of magnitude smaller than the peak height. For computer simulations, the FWM is better to work with because it has a simpler form, and fewer calculations are required. For this reason, the FWM will be used in the next chapter for comparisons to other waves.

Chapter 4

Comparison With Other Waves

Having established the possibility of launching localized waves from a finite array, the next step is to compare these waves to others. The FWM will be compared to continuous waves as well as to X waves. The FWM pulse should propagate without diffracting farther than the continuous waves, which would give them increased resolution when used for ultrasound imaging. The question is how far a FWM will propagate when generated from a realistic array, since the propagation distance is dependent on array size. The propagation characteristics of the FWM should be similar those of the X waves, as they are both localized waves, or limited diffraction beams.

To make the comparisons, the variables and parameters for the FWM must have dimensions reintroduced. In the interest of making a fair comparison, comparable continuous waves and X waves must be chosen.

4.1 Continuous Waves

4.1.1 Making a Fair Comparison

Continuous waves are defined by their wavelength, so in order to compare localized waves to continuous waves, a comparable value for the wavelength of the continuous wave must be chosen. This is somewhat nontrivial, as the localized waves are not sharply defined by a single wavelength. Rather, they have a broad spectrum, which must be measured somehow and converted to a wavelength.

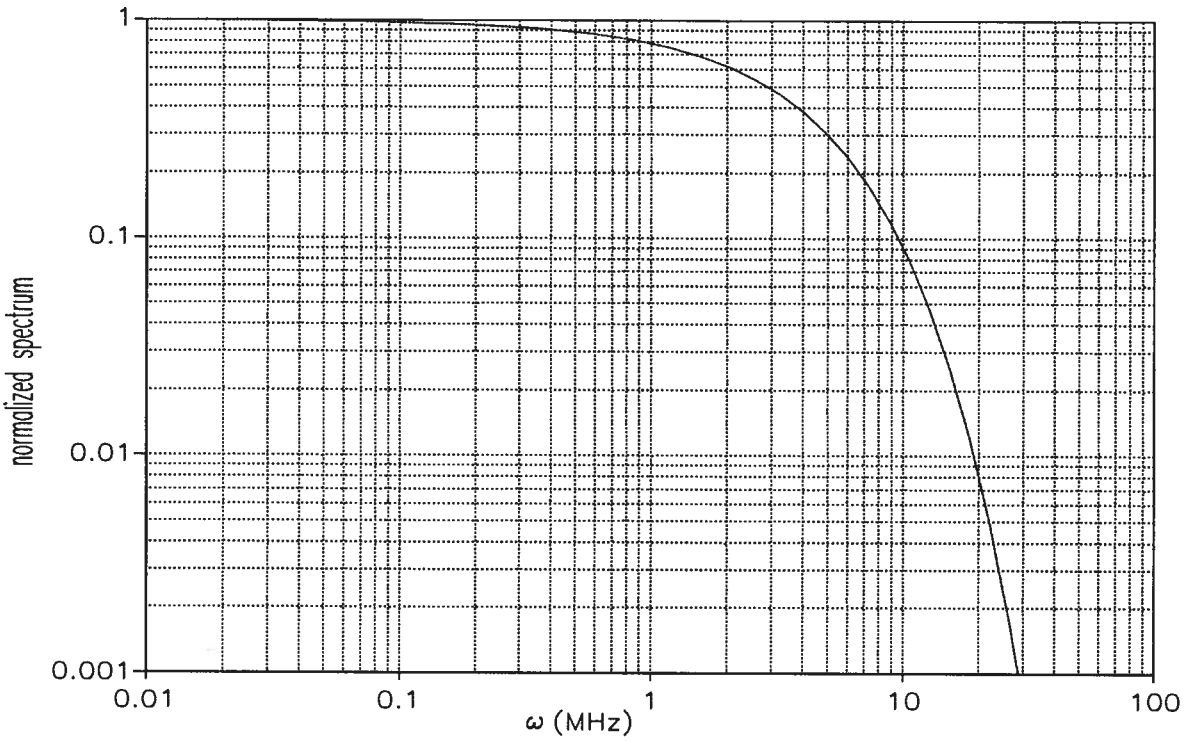

Figure 4.17: FWM spectrum for parameters $z_0' = 9 \times 10^{-4}$ and $k = 2.5m^{-1}$.

Focus Wave Mode Spectrum

The temporal Fourier transform of the focus wave mode at the origin is given by:

$$\begin{aligned} \mathcal{F}\{\phi(\vec{r} = \vec{0}, t)\} &= \\ \Phi(\vec{r} = \vec{0}, \omega) &= \begin{cases} \frac{1}{c} e^{-\frac{z_0'}{kc}(\omega - kc)} & \omega \geq kc \\ 0 & \omega < kc \end{cases} \end{aligned} \tag{4.30}$$

Figure 4.17 shows the spectrum for the FWM with parameters $z_0' = 9 \times 10^{-4}$ and $k = 2.5m^{-1}$. The speed of sound in water, c, is $1.5 \times 10^3 m/s$.

The spectrum of the FWM can be used to select a comparable continuous wave, as well as the parameter k to dimensionalize the pulse and array discussed previously. If a cut-off frequency, ω_p, is defined as the frequency before which the fraction p of the

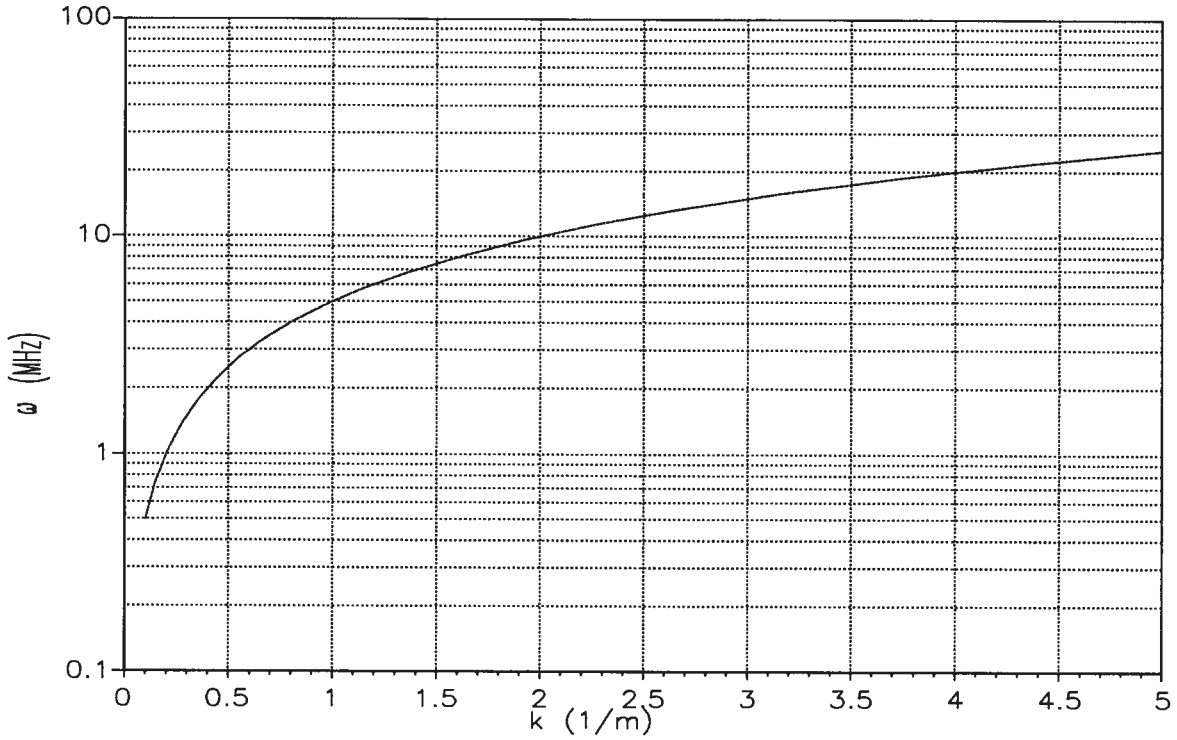

Figure 4.18: ω_p vs k for $p = 0.95$

spectrum is contained, that is:

$$\frac{\int_{-\infty}^{\omega_p} \Phi(\vec{r} = \vec{0}, \omega) d\omega}{\int_{-\infty}^{\infty} \Phi(\vec{r} = \vec{0}, \omega) d\omega} = p \tag{4.31}$$

then ω_p is calculated as:

$$\omega_p = kc \left(1 - \frac{\ln(1-p)}{z_0'}\right) \tag{4.32}$$

Figure 4.18 shows the variation of cut-off frequency, ω_p, as a function of k. The values of z_0' and c are as given previously.

Conversely, if the cut-off frequency and the fraction of the integral of the spectrum defining that frequency are determined, then the parameter k can be found and used to

give dimensions to the array and the FWM pulse as follows:

$$k = \frac{\omega_p}{c}\left(\frac{z_0'}{z_0' - \ln(1-p)}\right) \tag{4.33}$$

Having developed a method to select a comparable wavelength for the continuous wave, as well as a way to dimensionalize the FWM, the two can be compared.

4.1.2 Results

The behavior of a Gaussian beam propagating in free space in the z direction is as follows: if w_0 is the initial beam waist (at the $1/e$ point), and λ is the wavelength, then along the line of propagation, the amplitude varies as $1/[1 + (\lambda z/\pi w_0^2)^2]^{1/2}$. The beam half-width is also a function of z, and is expressed as (Arnaud, 1976):

$$w(z) = w_0\left[1 + \left(\frac{\lambda z}{\pi w_0^2}\right)^2\right]^{1/2} \tag{4.34}$$

The distance to the boundary between the near and far fields, that is the Rayleigh length, where the beam begins to decay as $1/z$ is reached when $z \approx \pi w_0^2/\lambda$. At that point, the amplitude has fallen to $1/\sqrt{2}$ times it's original value, and its radius has increased to $\sqrt{2}w_0$. in the region $z > \pi w_0^2/\lambda$, the beam diverges at an angle which can be approximated by $\theta \approx \lambda/(\pi w_0)$. The radius of the beam, therefore, increases as θz.

If the frequency of the Gaussian beam is chosen so that $f = \omega_p/2\pi$, then, inserting Equation (4.32) into the relation $\lambda = c/f$ gives the following expression for the wavelength:

$$\lambda = \frac{2\pi z_0'}{k(z_0' - ln(1-p))} \tag{4.35}$$

For the FWM, the value at the pulse center ($u = 0$) is given by:

$$\phi(\rho, u = 0, v = 2z) = e^{\frac{-k^2\rho^2}{z_0'}}\frac{e^{ikv}}{z_0'} \tag{4.36}$$

which defines the waist as $w_0 = (z_0'/k^2)^{1/2}$. Using this value for the initial waist of the Gaussian beam gives a Rayleigh length of:

$$L_R = \frac{\pi w_0^2}{\lambda} = \frac{z_0' - ln(1-p)}{2k} \tag{4.37}$$

Inserting this relation into the equation describing the waist of a Gaussian beam gives:

$$w = \frac{\sqrt{z_0}}{k}\left[1 + \left(\frac{2kz}{z_0' - ln(1-p)}\right)^2\right]^{1/2} \tag{4.38}$$

Both w and z can easily be nondimensionalized in the same way as the coordinates used in the localized wave investigation through multiplication by k, making the the new coordinates $w_1 = kw$ and $z_1 = kz$. With these coordinates, the beam waist is described by:

$$w_1 = \sqrt{z_0'}\left[1 + \left(\frac{2z_1}{z_0' - ln(1-p)}\right)^2\right]^{1/2} \tag{4.39}$$

Also, with these coordinates, the Rayleigh length is $L_{R1} = kL_R = [z_0' - ln(1-p)]/2$. For $z_0' = 9 \times 10^{-4}$ and $p = 0.95$, the dimensionless Rayleigh length evaluates to 1.5. This corresponds to a value for v_1 of $2L_{R1} = 3.0$. For the FWM created from the array studied in Section 3.2.2, there is no sign of diffractive spreading well past this point. In fact, out to $v_1 = 8\pi$ there is no spreading. For a distance of $z_1 = v_1/2 = 4\pi$, the waist of the Gaussian beam would have increased to over eight times its original size.

Results Using Realistic Arrays Using arrays of the size discussed previously, it is certainly possible to produce a localized wave that will outperform a Gaussian beam. What must now be considered are the results using smaller, more realistic arrays. To do this, dimensions must be reintroduced. Consider a Gaussian beam with a frequency of $f = 2$ MHz, which is within the ultrasound range of $1 - -15$MHz. For this cut-off frequency and a value for p of 0.95, k is calculated to be $2.5m^{-1}$. As before, $z_0' = 9 \times 10^{-4}$, making the initial waist $w_0 = 12mm$.

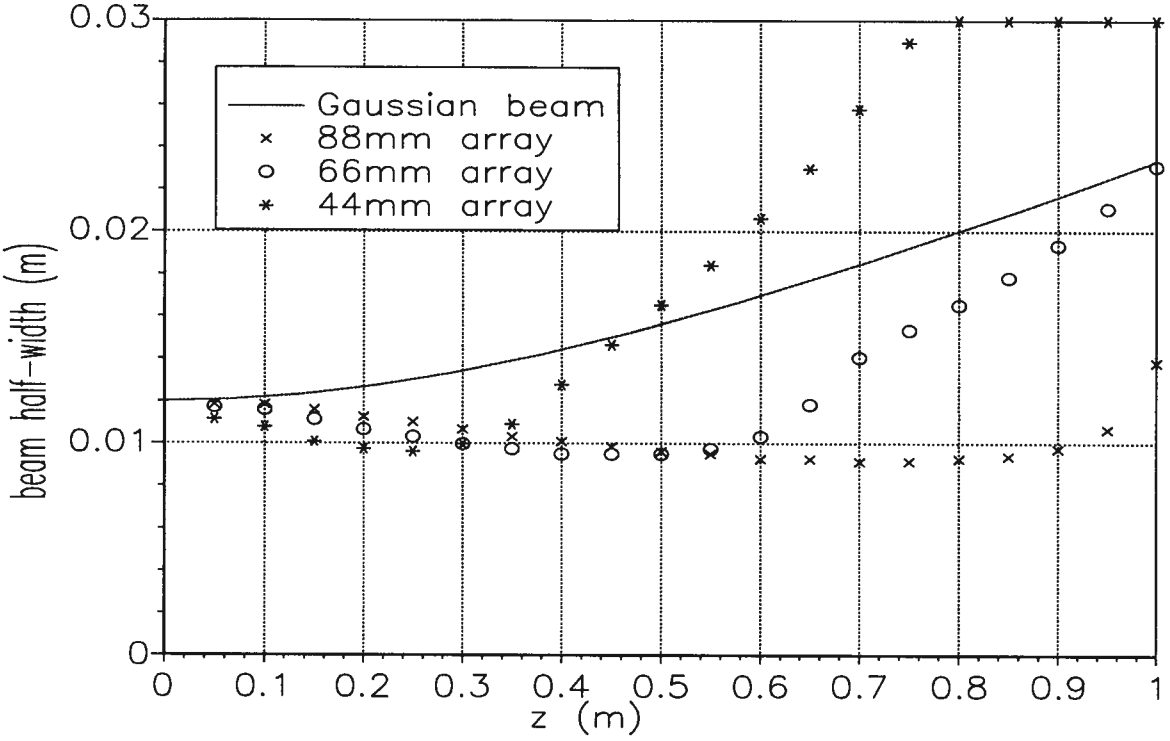

Figure 4.19: Half-width as a function of propagation distance for a Gaussian beam (solid line), and FWM beams generated from a $44mm \times 44mm$ array with 9×9 elements ($*$), $66mm \times 66mm$ array with 13×13 elements (o), and $88mm \times 88mm$ array with 17×17 elements ($\times$).

Three arrays of varying sizes are chosen to generate FWM pulses to compare with a Gaussian beam. In all three arrays, the element spacing is $5.5mm$, which is well above the lower bound for spacing set out in Section 3.3. The number of elements for each array is 9×9, 13×13, and 17×17, making the physical dimensions $44mm \times 44mm$, $66mm \times 66mm$, and $88mm \times 88mm$.

Figure 4.19 shows the theoretical half-width (at the $1/e$ point) as a function of propagation distance for a Gaussian beam as well as for $|\phi|$ produced by the three arrays. The value $|\phi|$ was chosen rather than simply charting the real part of the FWM in order to counter effects of the oscillatory nature of beam. As is expected, the larger array gives

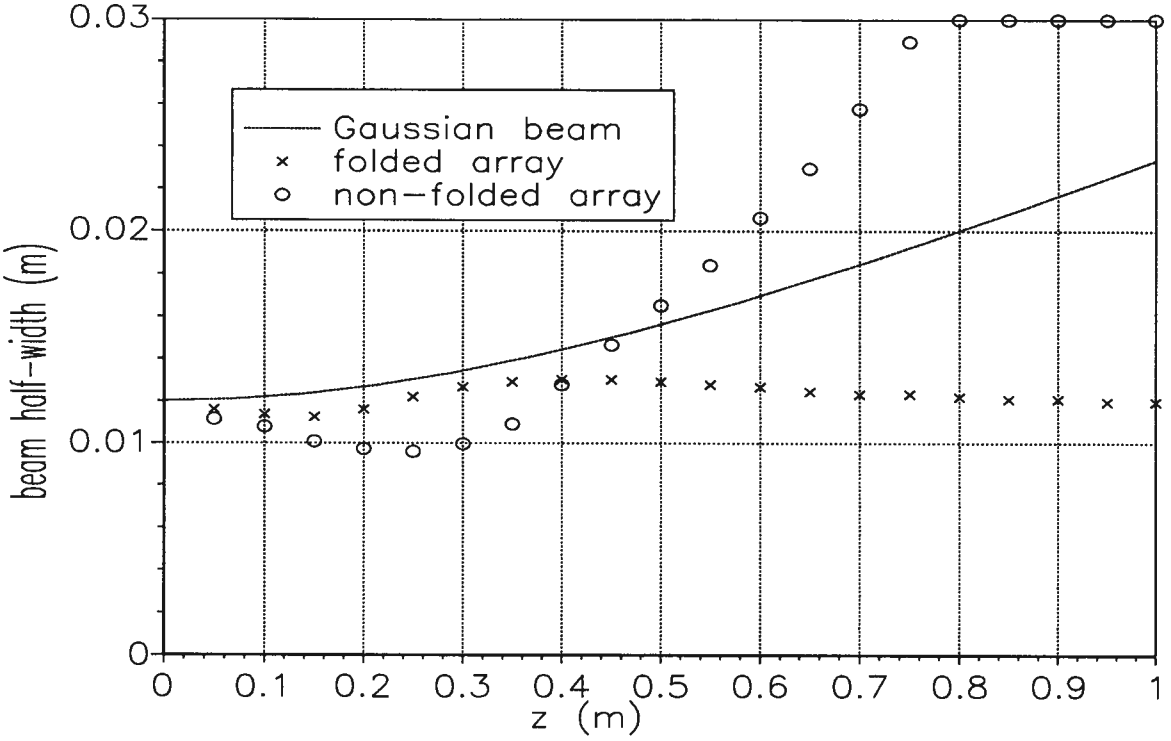

Figure 4.20: Half-width as a function of propagation distance for a Gaussian beam (solid line), and FWM beams generated from a $44mm \times 44mm$ array with 9×9 elements with ($\times$) and without (o) the folded term

the best results, showing much less diffraction than the Gaussian beam. For all arrays, the FWM beams show limited diffraction up to a distance of approximately ten times the array side dimension. For ultrasound use, the waves likely will not have to travel farther than $0.4m$, and all the FWM beams showed limited diffraction to that distance.

For the smallest array ($44mm \times 44mm$), the half-width of $|\phi|$ as produced using source functions including the folded term was found as a function of propagation distance. Figure 4.20 shows that evolution compared with the half-width for the Gaussian beam and the FWM from the same array without the folded term. The beam generated by the folded array appears to propagate farther before spreading, but closer inspection of the reconstruction shows that the folded array also seems to cause a lot of reconstruction

error. Figure 4.21 shows the lateral and axial plots of the reconstructed beam at $0.2m$ and $0.3m$ for both the folded and non-folded arrays. These are distances that an ultrasound beam will likely have to travel, and this plot shows the beam from the non-folded array to have much less reconstruction error. The folded array has a great deal of interference which shows up especially well in the lateral beam plot. Through the important range for ultrasound imaging, up to $0.4m$, the reconstruction from the non-folded array actually has a narrower beam half-width. This coupled with the smoother reconstruction makes the non-folded source functions a better choice than the folded configuration.

At $z = 0.3m$, the half-width of the Gaussian beam has expanded to $13mm$, as calculated using Equation (4.34). For the two smallest arrays considered, the beam half-width of the FWM, taken from Figure 4.19, is $10mm$. This is a reduction of 23%, which should translate to a significant increase in resolution.

4.2 X Waves

Lu and Greenleaf have investigated the possibility of launching X waves using a finite aperture radiator (Lu and Greenleaf, 1992a). Like the focus wave mode solutions, the X waves will travel to infinite distance without spreading if they are produced by an infinite aperture. They found that even when produced by a finite aperture, the X waves will propagate large distances without spreading. They used the depth of field, the distance in the direction of propagation where the beam fell to half of its original value, to describe how far the beam produced from a finite aperture would travel without spreading. They found that the depth of field was a function of the size of the radiator, as is the case with the FWM results. They developed an expression for the depth of field, Z_{max}, as follows (Lu and Greenleaf, 1992a):

$$Z_{max} = \frac{D}{2} \cot \zeta \tag{4.40}$$

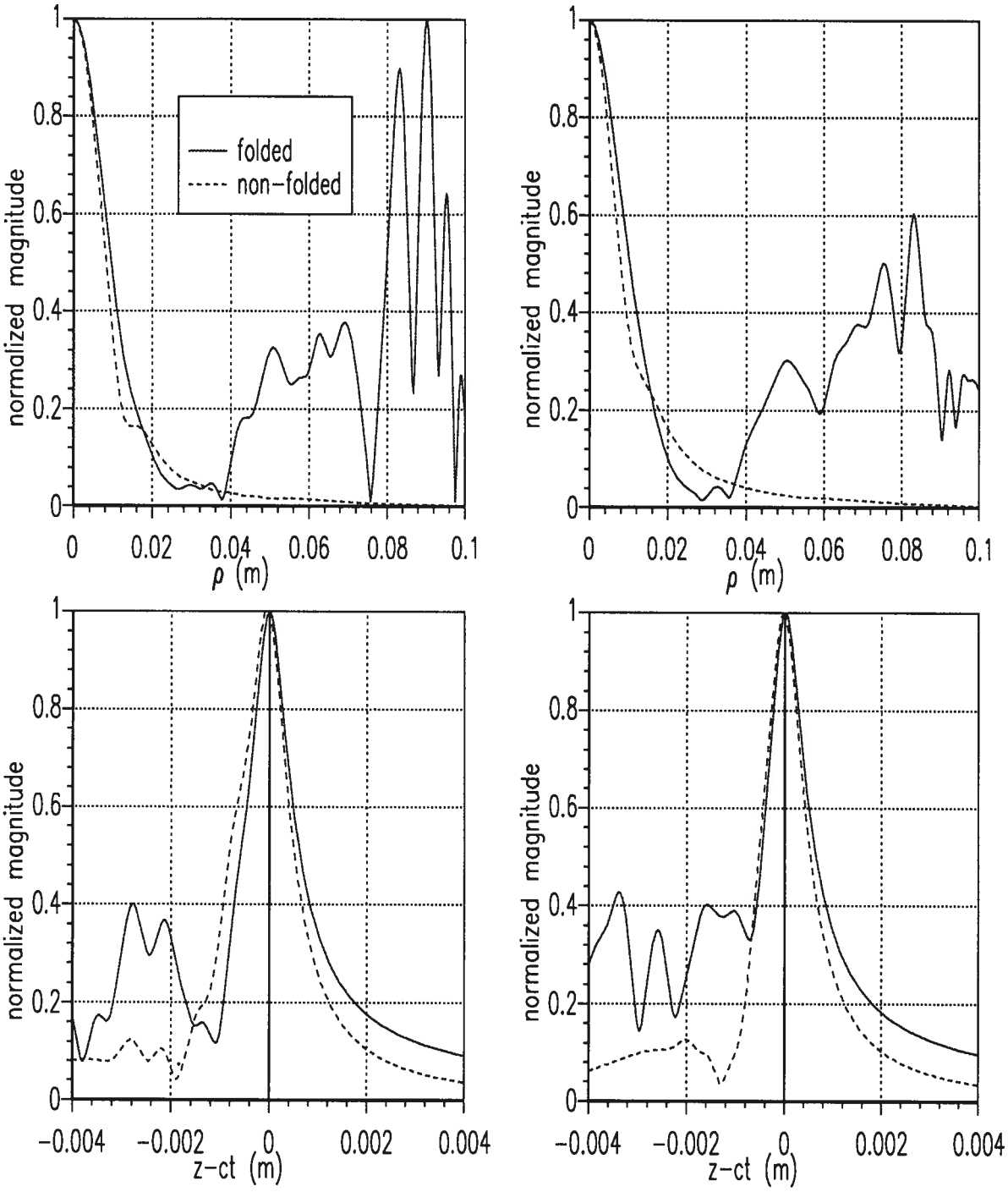

Figure 4.21: Lateral and axial plots of the reconstructed FWM at $0.2m$ (left) and $0.3m$ (right) from a 9×9 element $44mm \times 44mm$ array with (solid line) and without (dashed line) the folded term.

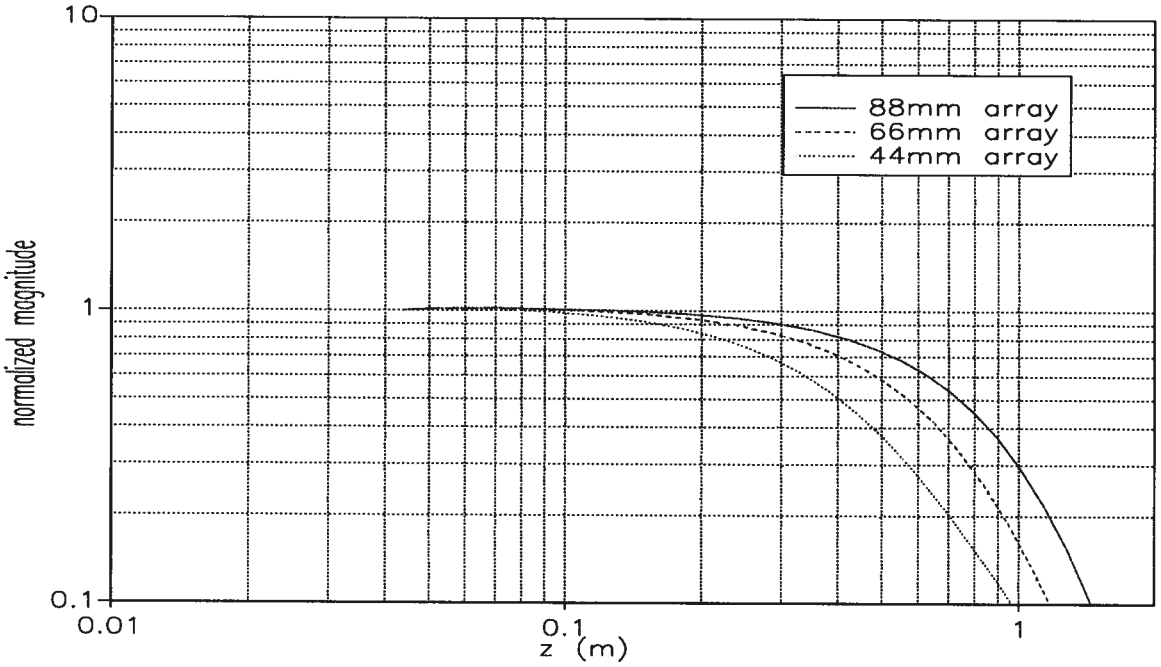

Figure 4.22: Evolution of $|\phi|$ for FWM beams generated from a $44mm \times 44mm$ array with 9×9 elements (dotted line), $66mm \times 66mm$ array with 13×13 elements (dashed line), and $88mm \times 88mm$ array with 17×17 elements (solid line).

where D is the diameter of the radiator, and ζ is the Axicon angle, which is a parameter affecting the lateral resolution. The X waves differ from the FWM in that the X wave peak value does not oscillate, but rather remains constant.

To evaluate the FWM pulses using the same criterion as the X waves, the value of $|\phi|$ as a function of the z was charted for the arrays of the previous section ($44mm \times 44mm$ with 9×9 elements, $66mm \times 66mm$ with 13×13 elements, and $88mm \times 88mm$ with 17×17 elements) in Figure 4.22. For the $44mm \times 44mm$ array, the depth of field, as defined in the previous paragraph, was found to be $405mm$, for the $66mm \times 66mm$ array a value of $573mm$ was found, and $744mm$ for the $88mm \times 88mm$ array.

For a full description of the X waves and their behavior when launched from a finite aperture, the reader is referred to (Lu and Greenleaf, 1992a). Their results for a $50mm$

diameter radiator, and an Axicon angle of 4° will be quoted here.

For a $50mm$ diameter radiator, Lu and Greenleaf found a depth of field of $358mm$, which is very close to the theoretical value of $357.6mm$ calculated from Equation (4.40). A $50mm$ diameter round radiator has the same area as the square $44mm \times 44mm$ array, making the two radiators comparable. The FWM has a depth of field of $405mm$, which is slightly better than that for the X-wave, but it is of the same order of magnitude, making the FWM is comparable behavior to the X wave.

If there were no cost or technological limits placed on the size of the generating array, a FWM beam could be generated that would handily outperform continuous waves of a comparable wavelength. Even with an array of currently realizable size and element spacing, the FWM generated will propagate through the important range for medical ultrasound imaging (up to about $0.4m$) with less diffractive spreading than continuous waves. This reduction in spreading is important in terms of image resolution. The propagation characteristics of the FWM are similar to another limited diffraction beam, X waves, in terms of propagation distance before the pulse falls to half its maximum value.

Chapter 5

Conclusions and Future Directions

In order to launch an exact replication of a localized wave, theory dictates that an infinite aperture is required. It is possible to generate a reasonable approximation using a finite array of discrete sources. The waves launched from a finite array do not exhibit the same propagation characteristics as those from an infinite aperture in that they will not propagate to infinity without experiencing decay or diffraction. They do, however, travel an extended distance before diffraction occurs.

The size of the generating array determines the length of this diffraction-limited period. The element spacing affects the smoothness in the area around the pulse center of the reconstructed wave, especially the trailing wake. The distance to which the wave will propagate varies linearly with the size of the array, so a square array who's side dimension is increased ten times (increasing the area one hundred times) will cause the wave to propagate ten times farther. The required element spacing does not change with reconstruction distance. This means that in order to generate beams which propagate greater distances, the array must be made larger by adding elements rather than by increasing the element spacing.

Since it is the array size that limits propagation distance, it is desirable to have a large array. A 'folding' scheme has been proposed to make a small array act like a larger array (Ziolkowski, 1989). Localized waves generated using this folded array do travel farther than their non-folded counterparts, but as the distance from the array increases, the quality of the wave decreases. There is greater reconstruction error in the area

surrounding the pulse center of the beam. Also, the source functions required for the folded term are much more complicated and three orders of magnitude larger than for the non-folded term. This, coupled with the fact that ultrasound waves are not required to travel great distances, diminishes the importance of the folded array configuration for this application.

It was previously thought that the infinite energy of the original FWM made it impossible to launch, and that finite energy variations on this wave must be found. Since the size of the generating array determines propagation limits rather than the waveform applied, the FWM can be launched from an array with the same success as its finite energy derivatives such as the MPS pulse. The difference between the normalized FWM and MPS pulse is two orders of magnitude smaller than the peak height. The FWM has a simpler formulation, which makes it preferable to work with over the MPS pulse, at least for simulations.

In a comparison with a traditional Gaussian beam using beam half-width at the $1/e$ point as a figure of merit, FWM beams generated by realistic arrays showed superior propagation characteristics through the area of interest (up to $0.4m$). This is an important measure of the wave in that it relates to the resolution of the resulting image. At a distance of $0.3m$ from the source array, the FWM has a beam half-width of $10mm$, while that of a comparable Gaussian beam is $13mm$. This is a reduction of 23% for the FWM.

Compared to X waves, another limited diffraction beam, the FWM showed similar propagation characteristics. The criterion used in this comparison was the distance the beam traveled before falling to half its original magnitude. When generated from arrays of the same area, the FWM traveled slightly farther than the X wave, $405mm$ as opposed to $358mm$.

Future Directions Real transducer behavior and how it might limit the source functions was not considered. An investigation into this could yield important information. The simulations showed that there was little difference between the reconstructed FWM and MPS pulse, however an analysis of the source functions for both could help determine which waveform should be used. The folded source functions could also be analyzed.

The application of windowing techniques could be studied. The effect of applying a Hanning or Hamming window the size of the array was examined, but this type of window just made the array act like a smaller one. The use of temporal windows, or spatial windows the size of the individual elements could be investigated.

All of the results obtained here were through computer simulations. The next step would be to test these findings using a real transducer array. An entire array does not have to be built to accomplish this. Rather, a single transducer could be used, moving it to each location in the array, measuring the resulting signal, and adding the signals.

Bibliography

Arnaud, J. A. (1976). *Beam and Fiber Optics.* Academic Press, New York.

Brittingham, J. N. (1983). Focus waves modes in homogeneous Maxwell's equations: Transverse electric mode. *J. Appl. Phys.*, 54(3):1179–1189.

Durnin, J. (1987). Exact solutions for nondiffracting beams. I. the scalar theory. *J. Opt. Soc. Am. A*, 4(4):651–654.

Durnin, J., Miceli, Jr., J. J., and Eberly, J. H. (1987). Diffraction-free beams. *Phys. Rev. Lett.*, 58(15):1499–1501.

Fatemi, M. and Arad, M. A. (1992). A novel imaging system based on nondiffracting X waves. In McAvoy, B. R., editor, *IEEE Ultrasonics Symposium*, pages 609–612. Ultrasonics, Ferroelectric, and Frequency Control Society.

Goldberg, R. L., Smith, S. W., Ladew, R. A., and Brent, J. C. (1992). Multi-layer PZT transducer arrays for improved sensitivity. In McAvoy, B. R., editor, *IEEE Ultrasonics Symposium*, pages 551–554. Ultrasonics, Ferroelectric, and Frequency Control Society.

Greenleaf, J. F. (1983). Computerized tomography with ultrasound. *Proceedings of the IEEE*, 71(3):330–337.

Hillion, P. (1986). More on focus wave modes in Maxwell equations. *J. Appl. Phys.*, 60(8):2981–2982.

Hykes, D. L., Hedrick, W. R., and Starchman, D. E. (1992). *Ultrasound Physics and Instrumentation.* Churchill Livingstone Inc., New York, New York, second edition.

Jones, D. S. (1964). *The Theory of Electromagnetism.* Pergamon, New York.

Lu, J.-y. and Greenleaf, J. F. (1992a). Nondiffracting X waves—exact solutions to free-space scalar wave equation and their finite aperture realizations. *IEEE Trans. Ultrason. Ferroelec., and Freq. Contr.*, 39(1):19–31.

Lu, J.-y. and Greenleaf, J. F. (1992b). Steering of limited diffraction beams with a two-dimensional array transducer. In McAvoy, B. R., editor, *IEEE Ultrasonics Symposium*, pages 603–607. Ultrasonics, Ferroelectric, and Frequency Control Society.

Lu, J.-y., Song, T. K., Kinnick, R. R., and Greenleaf, J. F. (1993). In vitro and in vivo real-time imaging with ultrasonic limited diffraction beams. *IEEE Trans. Med. Imaging*, 12(4):819–829.

Macovski, A. (1983). *Medical Imaging Systems.* Prentice-Hall Inc., Englewood Cliffs, New Jersey.

Palmer, M. R. and Donnelly, R. (1993). Focused waves and the scalar wave equation. *J. Math. Phys.*, 34(9):4007–4013.

Smith, S. W. and Light, E. D. (1992). Two-dimensional array transducers using hybrid connection technology. In McAvoy, B. R., editor, *IEEE Ultrasonics Symposium*, pages 555–558. Ultrasonics, Ferroelectric, and Frequency Control Society.

Wu, T. T. (1985). Electromagnetic missiles. *J. Appl. Phys.*, 57(7):2370–2373.

Wu, T. T., King, R. W. P., and Shen, H.-M. (1987). Spherical lens as a launcher of electromagnetic missiles. *J. Appl. Phys.*, 62(10):4036–4040.

Ziolkowski, R. W. (1985). Exact solutions of the wave equation with complex source locations. *J. of Math. Phys.*, 26(4):861–863.

Ziolkowski, R. W. (1989). Localized transmission of electromagnetic energy. *Phys. Rev. A*, 39(4):2005–2033.

Ziolkowski, R. W. (1991). Localized wave physics and engineering. *Phys. Rev. A*, 44(6):3960–3984.

Ziolkowski, R. W. and Lewis, D. K. (1990). Verification of the localized-wave transmission effect. *J. Appl. Phys.*, 68(12):6083–6086.

Ziolkowski, R. W., Lewis, D. K., and Cook, B. D. (1989). Evidence of localized wave transmission. *Phys. Rev. Lett.*, 62(2):147–150.